South Florida deep convection: Convective initiation , cloud dynamics, microphysics, and anvil generation

William R. Cotton
Colorado State University
Dept. of Atmospheric Science
Fort Collins, CO

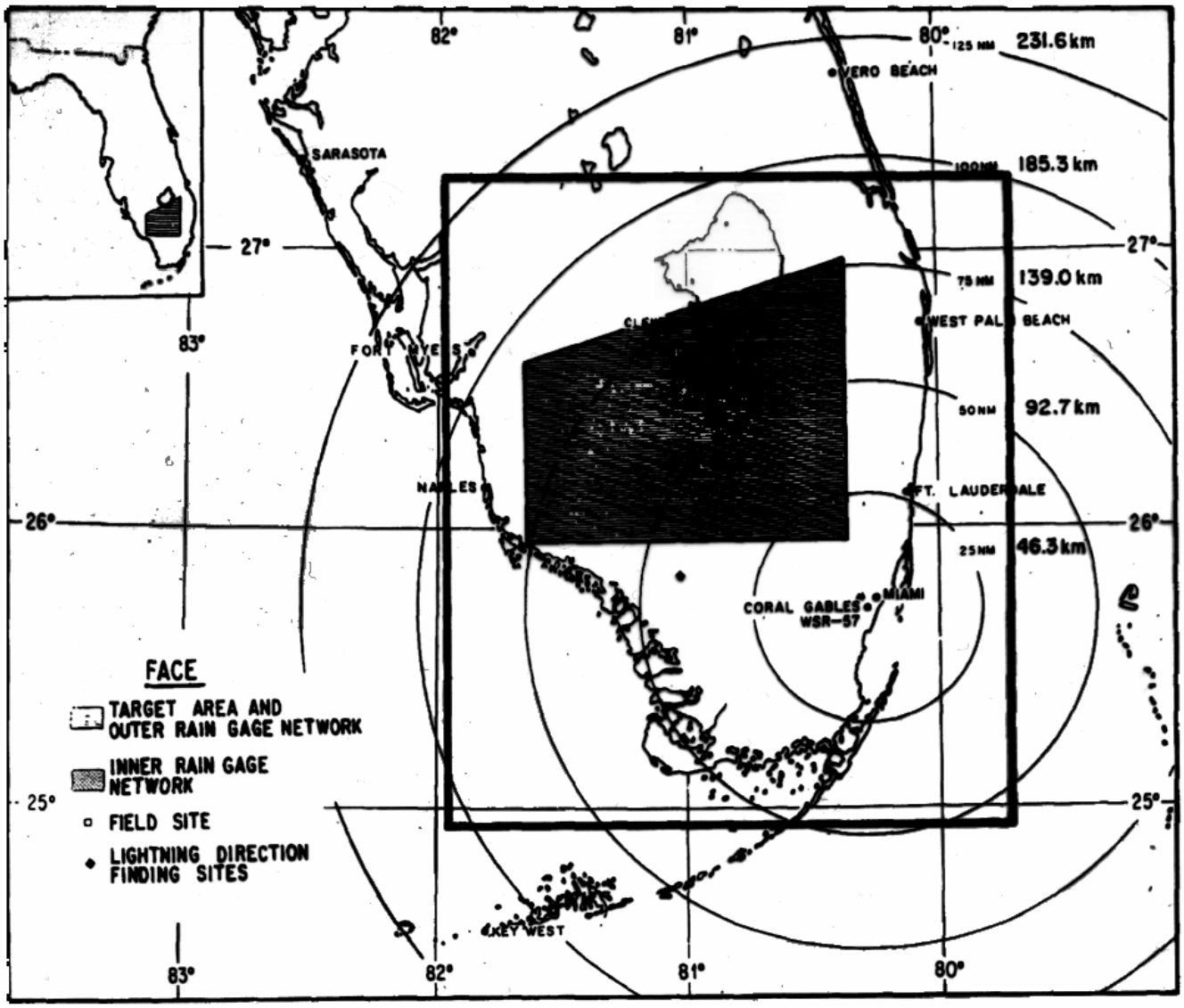

FIG. 1. Map of south Florida showing the FACE target area, the position of the WSR-57 radar, and the range marks from the radar. The heavy outline indicates the area for which radar data are presented.

Mesg-1

A UNITED STATES DEPARTMENT OF COMMERCE PUBLICATION

NOAA Technical Memorandum ERL OD-16

U.S. DEPARTMENT OF COMMERCE
NATIONAL OCEANIC AND ATMOSPHERIC ADMINISTRATION
Environmental Research Laboratories

An Observational Study of Cumulus Convection Patterns in Relation to the Sea Breeze Over South Florida

ROGER PIELKE

Office
of the Director
BOULDER,
COLORADO
January 1973

Southeast Wind Case

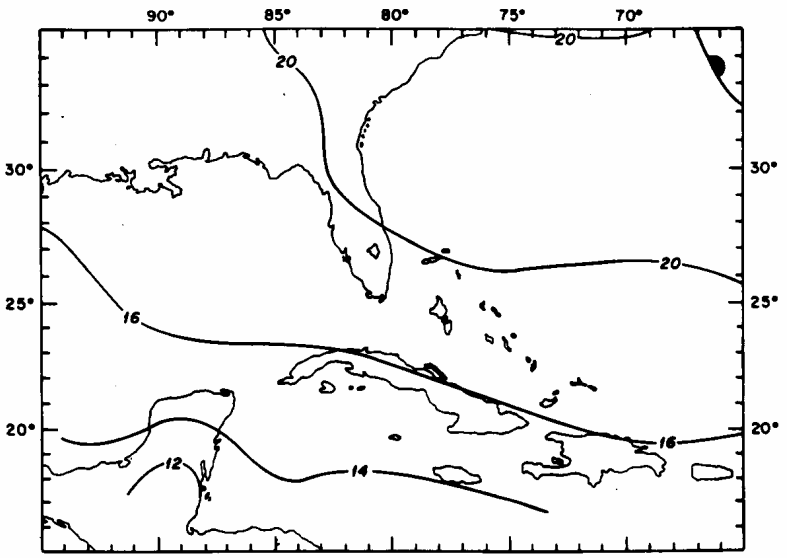

Figure 28. The surface analysis at 0700 EST on August 19, 1971.

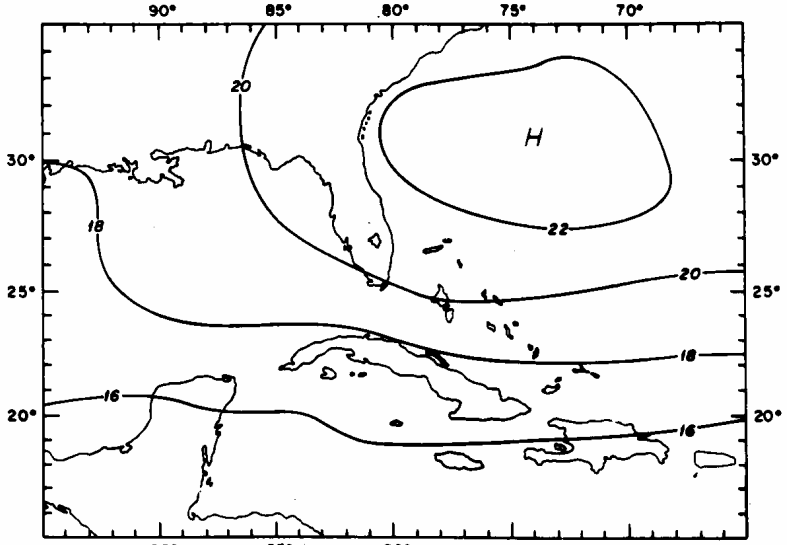

Figure 29. The surface analysis at 1300 EST on August 19, 1971.

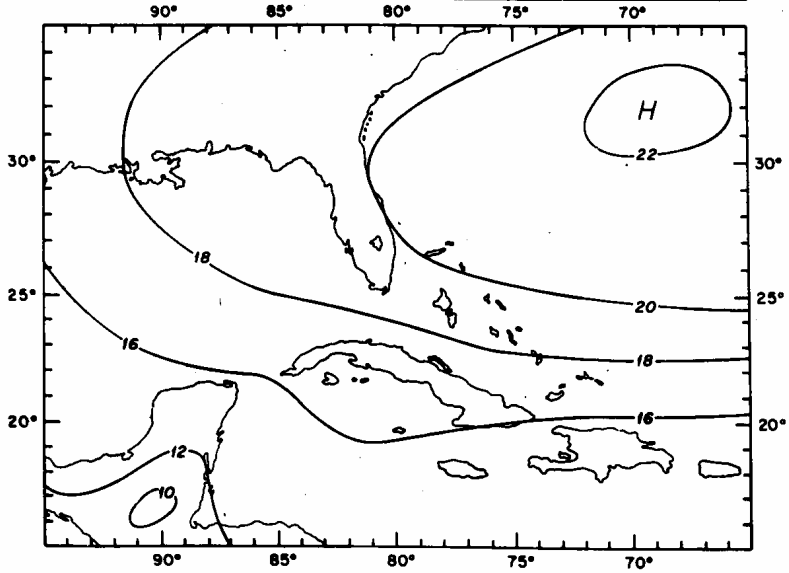

Figure 30. The surface analysis at 1900 EST on August 19, 1971.

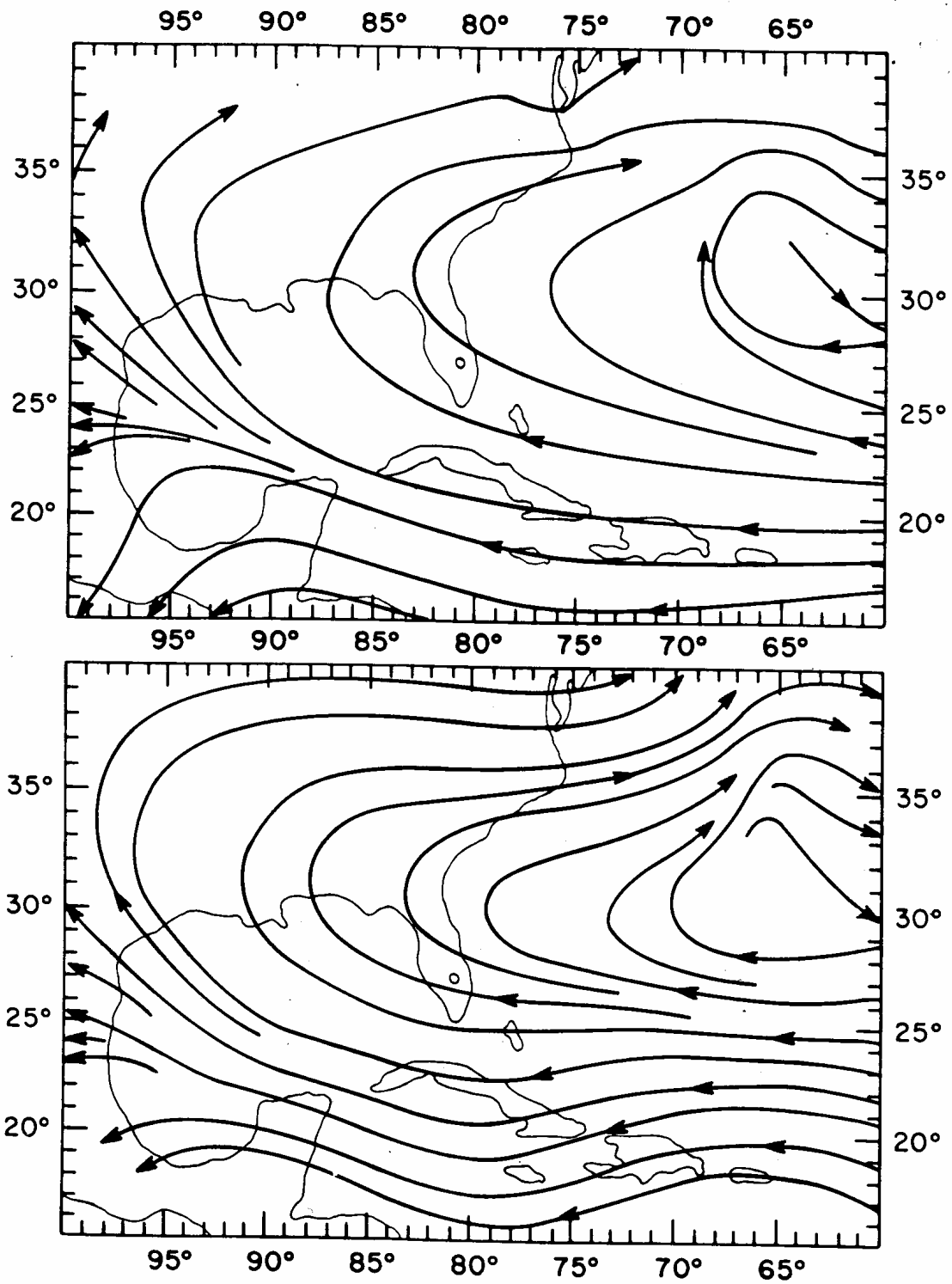

Figure 31. (top) Lower troposphere mean circulation 1000-600 mb layer at 0700 EST on August 19, 1971.

Figure 32. (bottom) Lower troposphere mean circulation 1000-600 mb layer at 1900 EST on August 19, 1971.

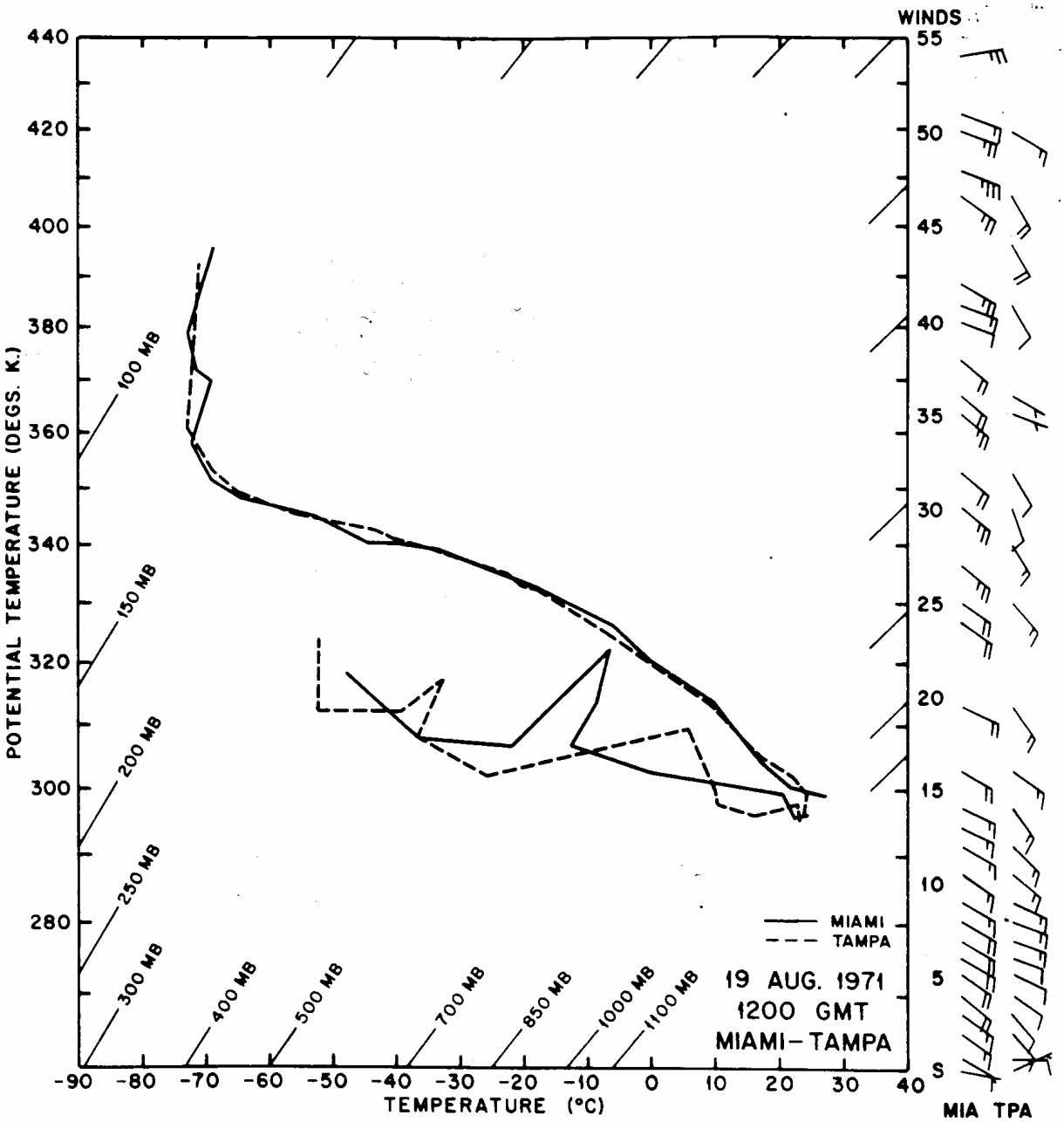

Figure 33. The radiosonde soundings at Miami and Tampa at 0700 EST on August 19, 1971.

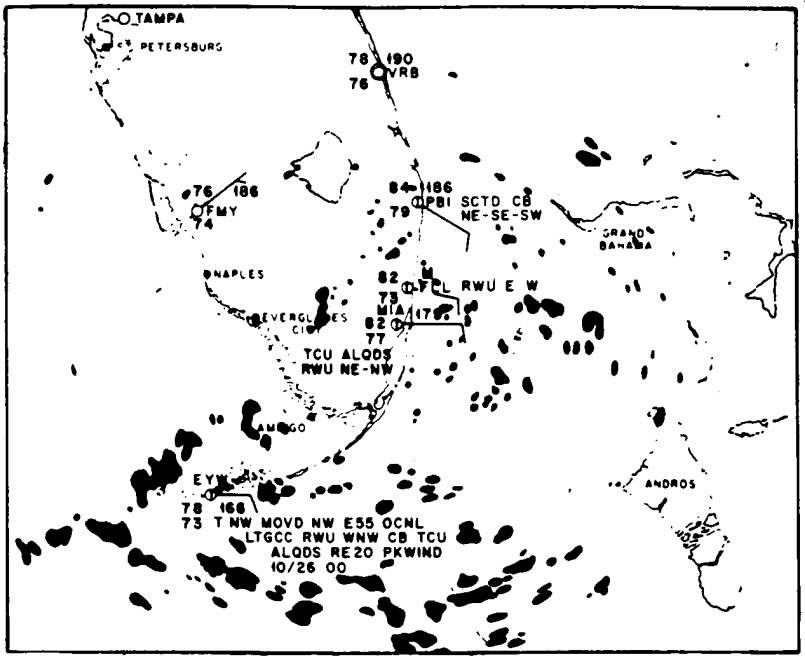

Figure 34. Miami WSR-57 radar echo coverage at 0655 EST and surface observations at 0700 EST on August 19, 1971.

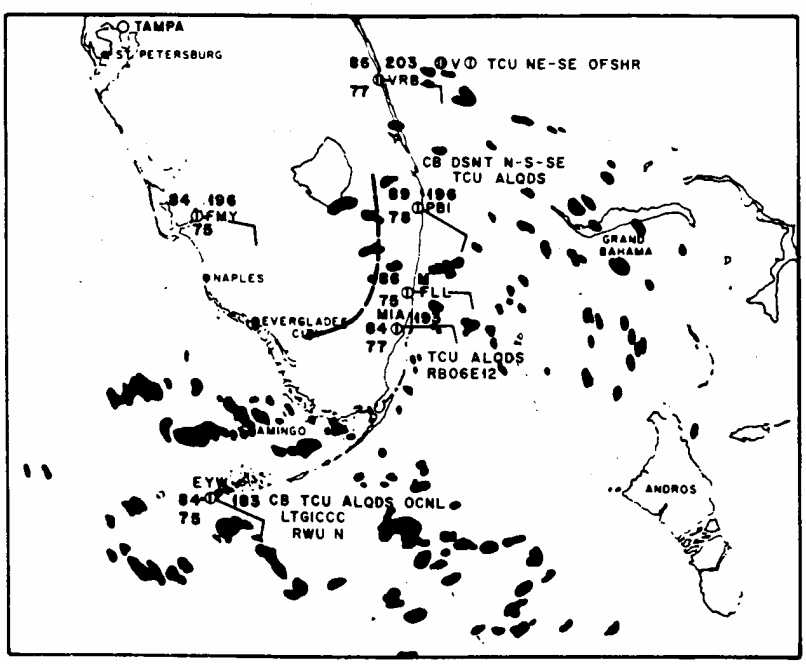

Figure 35. Miami WSR-57 radar echo coverage at 0905 EST and surface observations at 0900 EST on August 19, 1971.

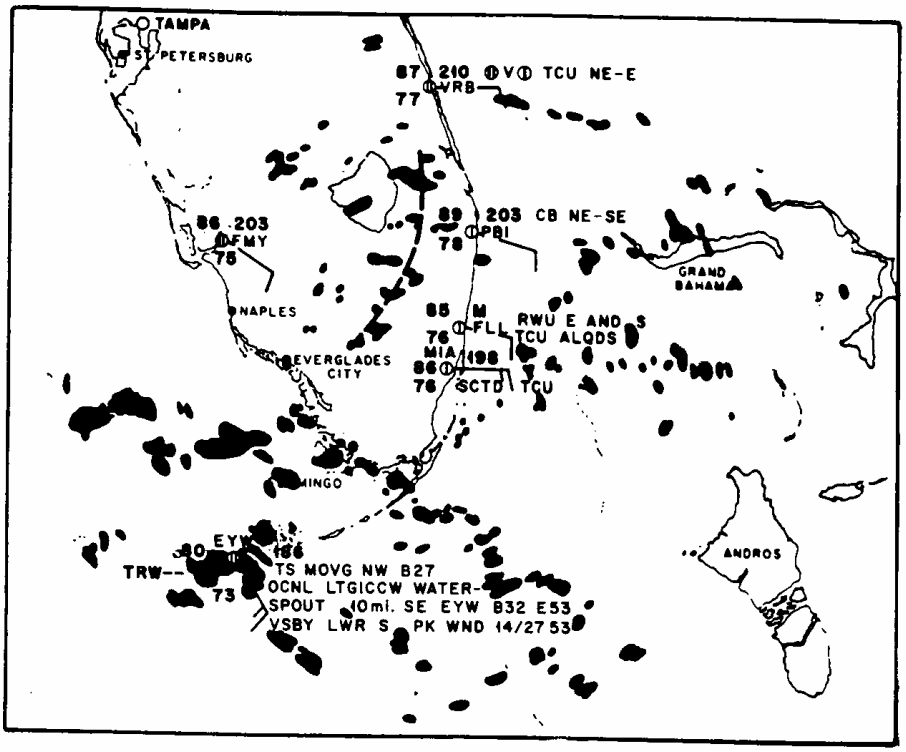

36. *Miami WSR-57 radar echo coverage at 1002 EST and surface observations at 1000 EST on August 19, 1971.*

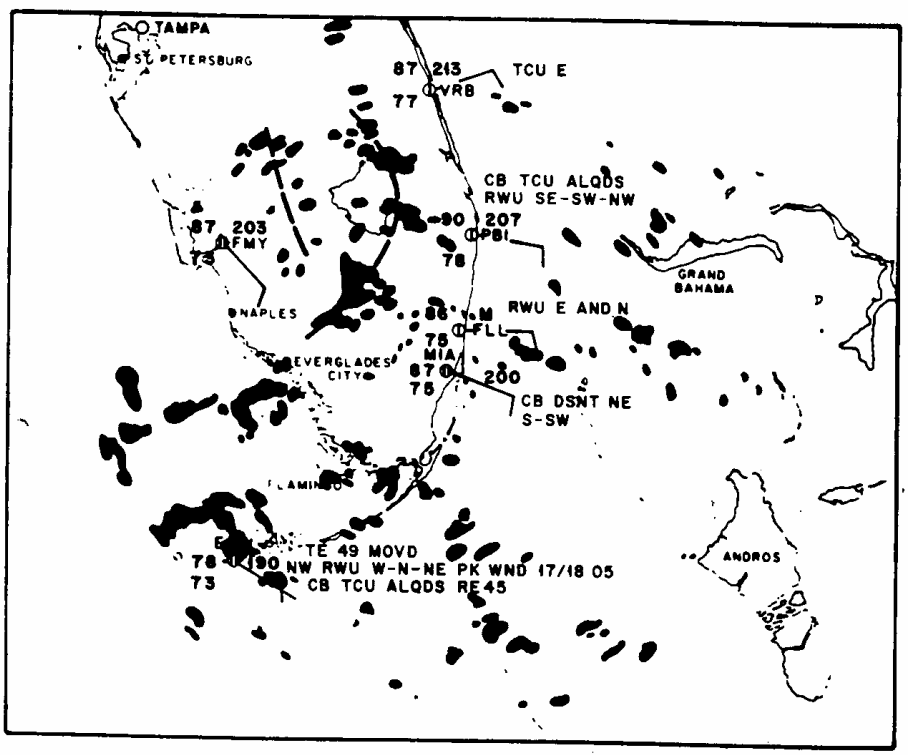

37. *Miami WSR-57 radar echo coverage at 1100 EST and surface observations at 1100 EST on August 19, 1971.*

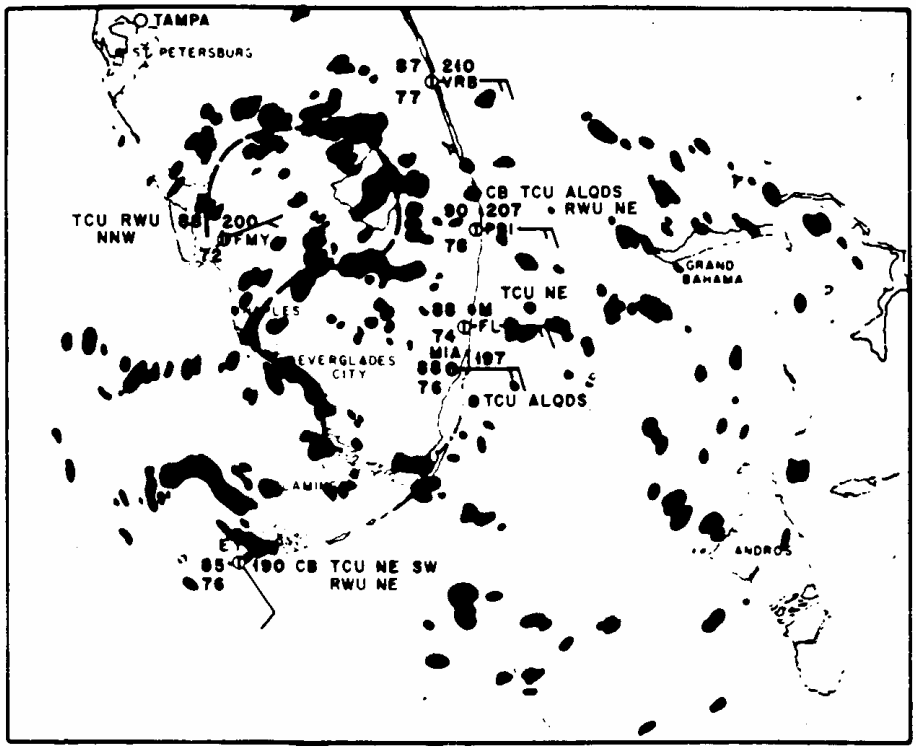

Figure 38. Miami WSR-57 radar echo coverage at 1202 EST and surface observations at 1200 EST on August 19, 1971.

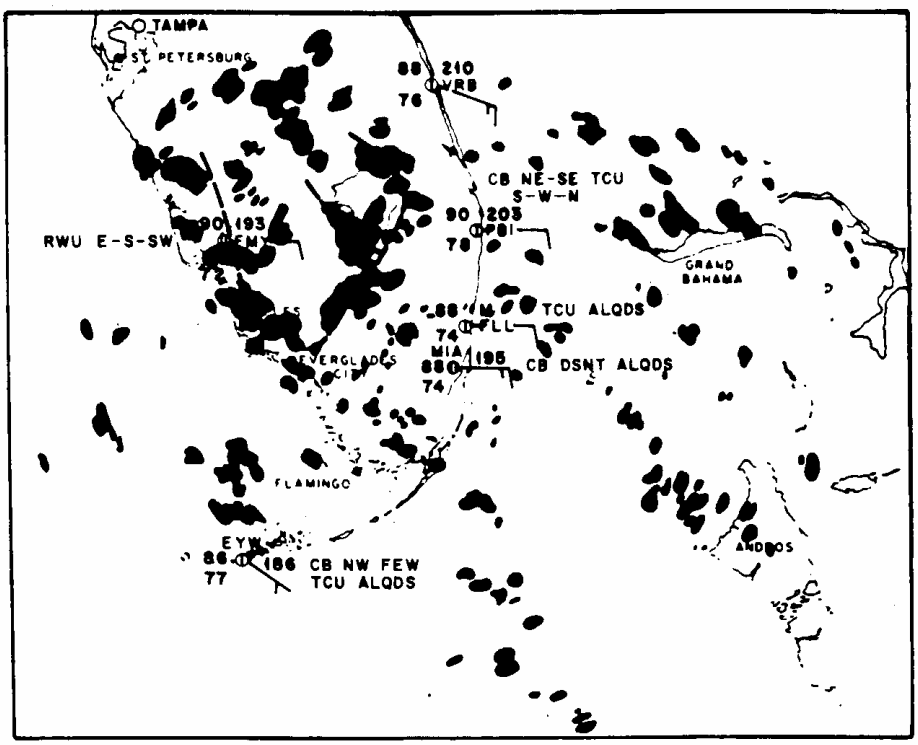

Figure 39. Miami WSR-57 radar echo coverage at 1301 EST and surface observations at 1300 EST on August 19, 1971.

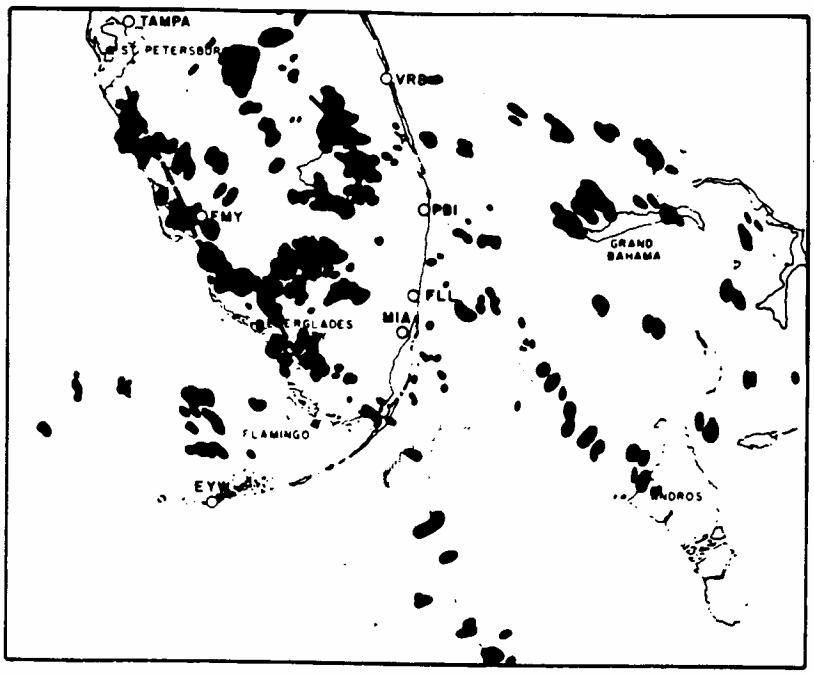

Figure 40. Miami WSR-57 radar echo coverage at 1333 EST on August 19, 1971.

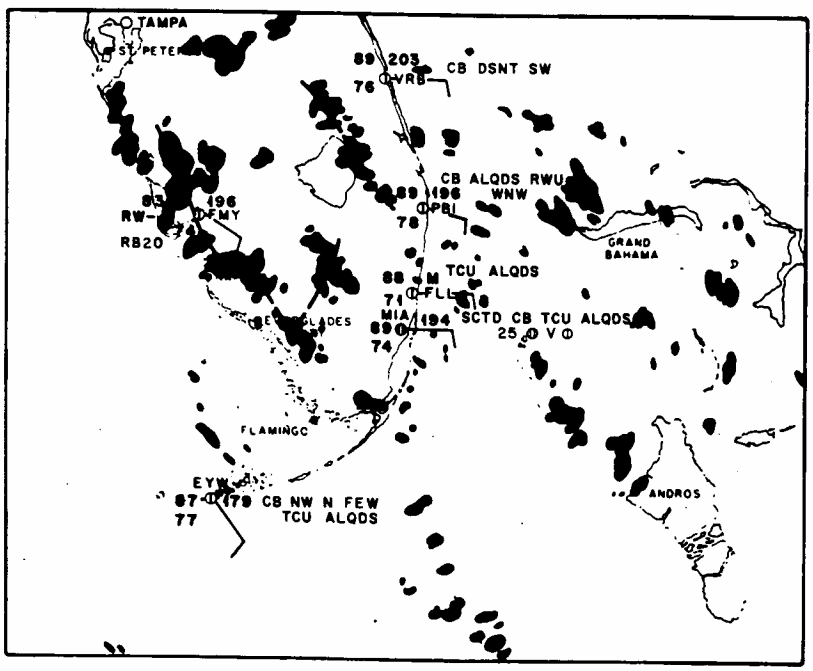

Figure 41. Miami WSR-57 radar echo coverage at 1402 EST and surface observations at 1400 EST on August 19, 1971.

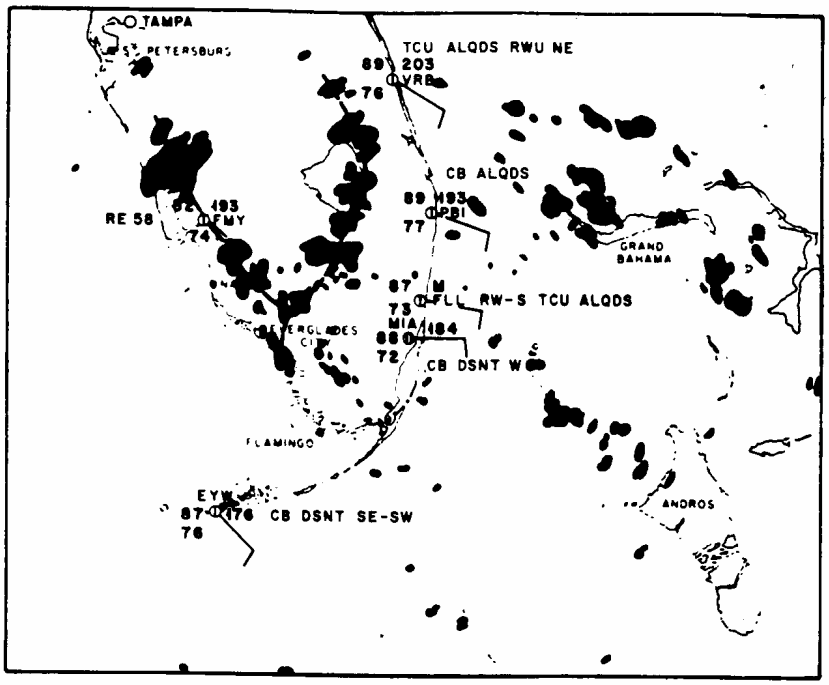

Figure 42. Miami WSR-57 radar echo coverage at 1501 EST and surface observations at 1500 EST on August 19, 1971.

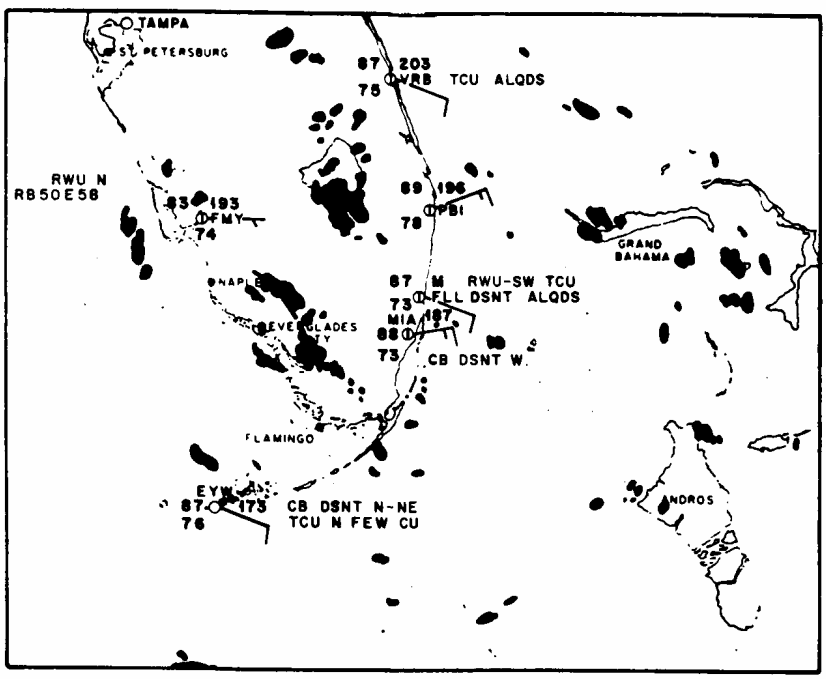

Figure 43. Miami WSR-57 radar echo coverage at 1559 EST and surface observations at 1600 EST on August 19, 1971.

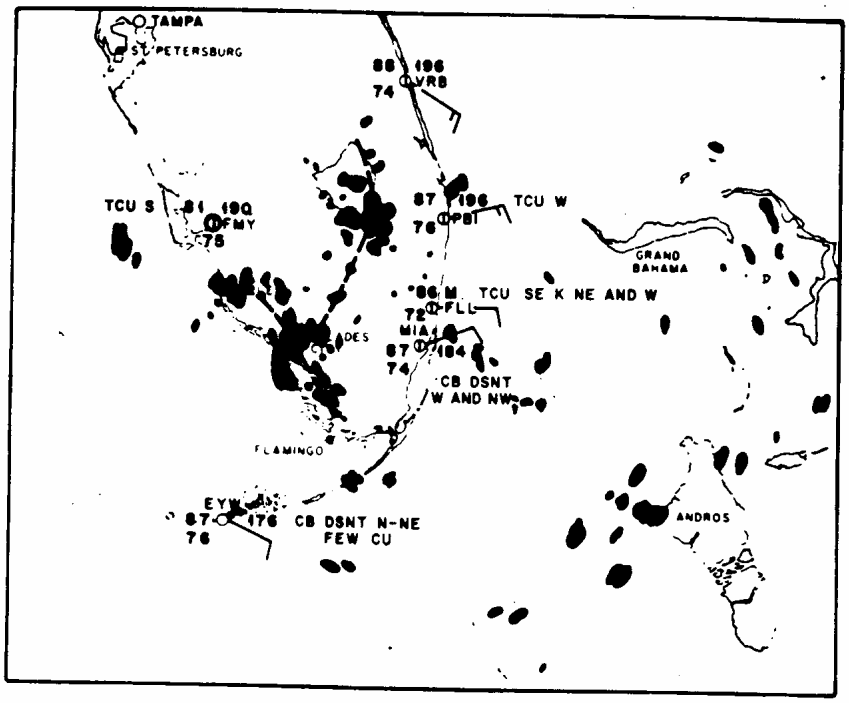

Figure 44. Miami WSR-57 radar echo coverage at 1702 EST and surface observations at 1700 EST on August 19, 1971.

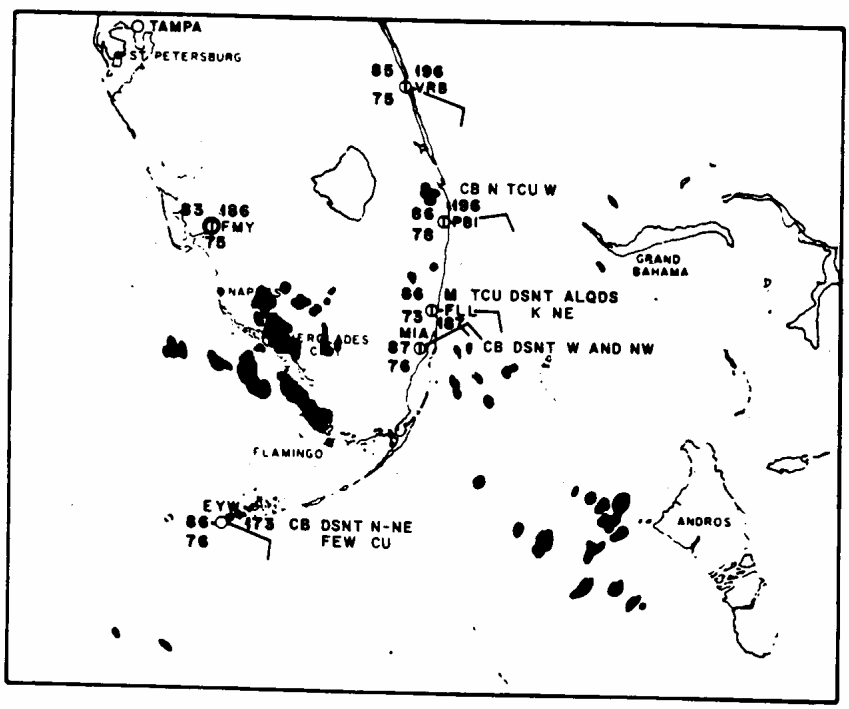

Figure 45. Miami WSR-57 radar echo coverage at 1802 EST and surface observations at 1800 EST on August 19, 1971.

Southerly wind case

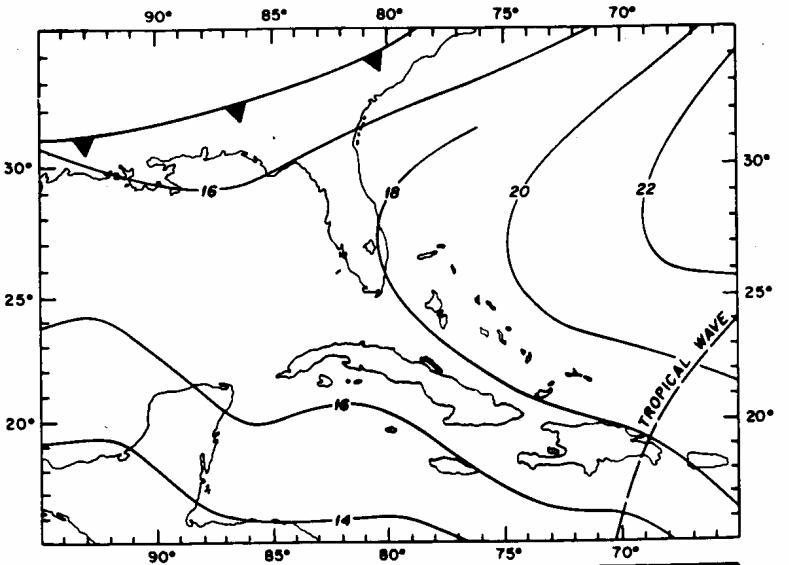

Figure 46. The surface analysis at 0700 EST on July 20, 1971.

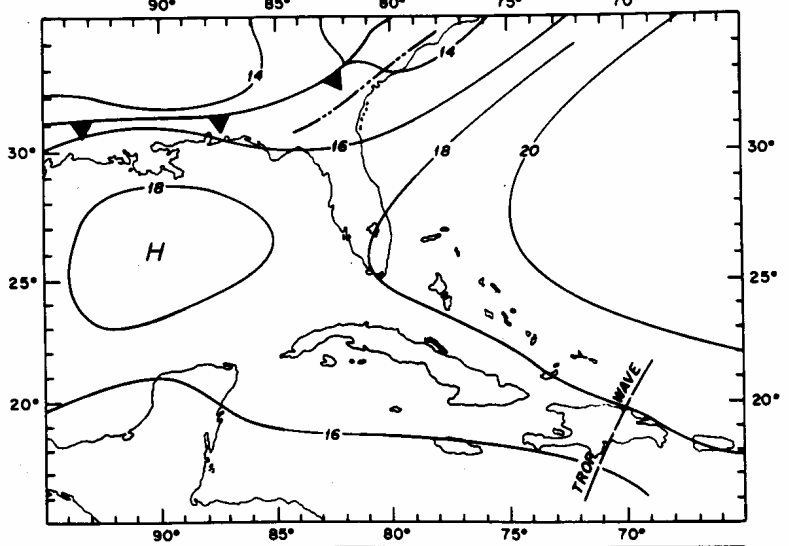

Figure 47. The surface analysis at 1300 EST on July 20, 1971.

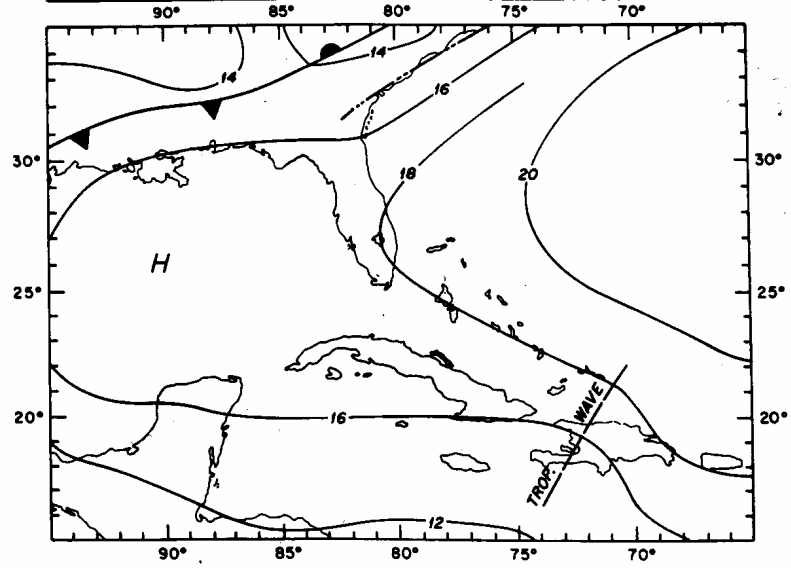

Figure 48. The surface analysis at 1900 EST on July 20, 1971.

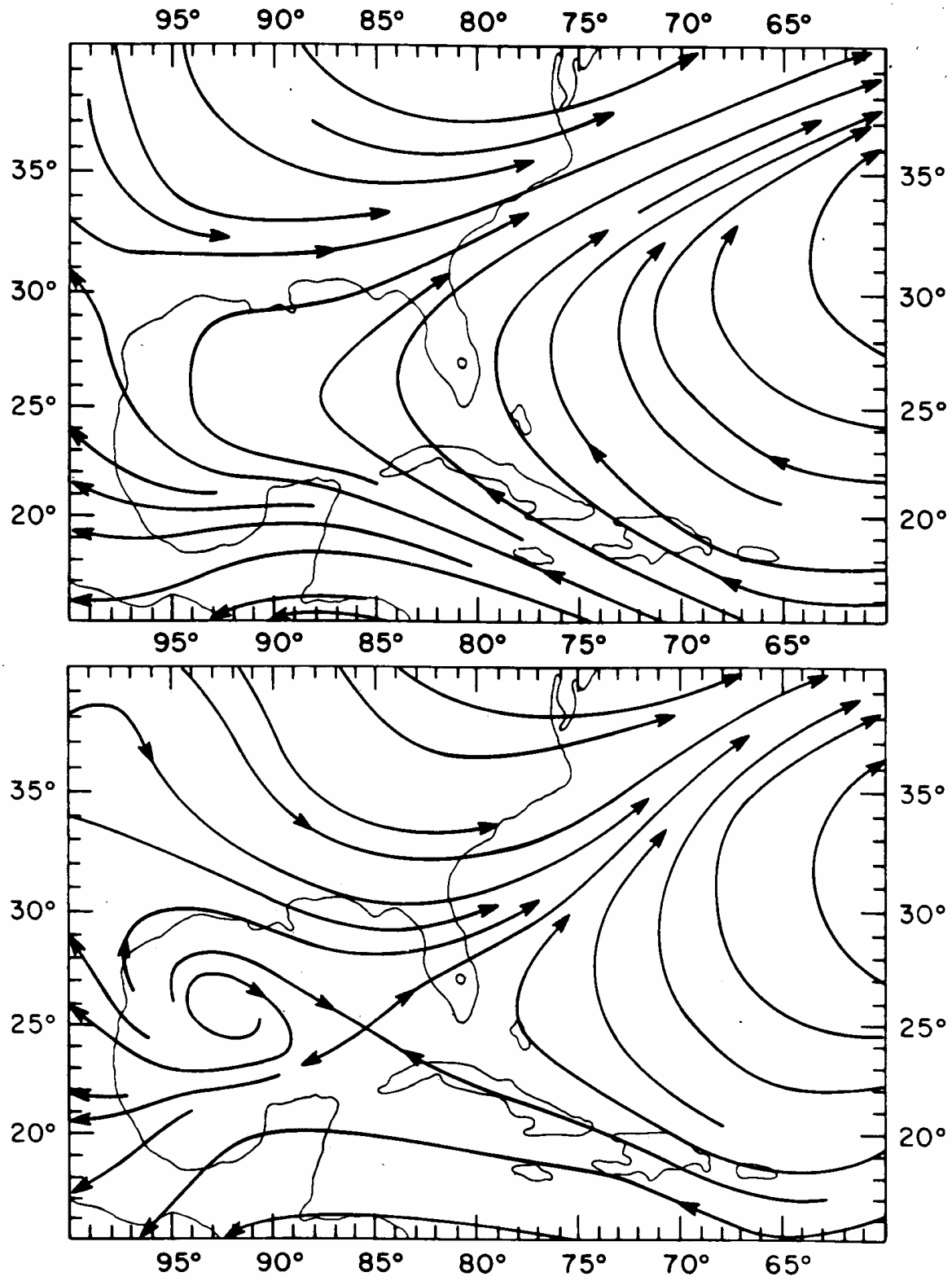

Figure 49. (top) Lower troposphere mean circulation 1000-600 mb layer at 0700 EST on July 20, 1971.

Figure 50. (bottom) Lower troposphere mean circulation 1000-600 mb layer at 1900 EST on July 20, 1971.

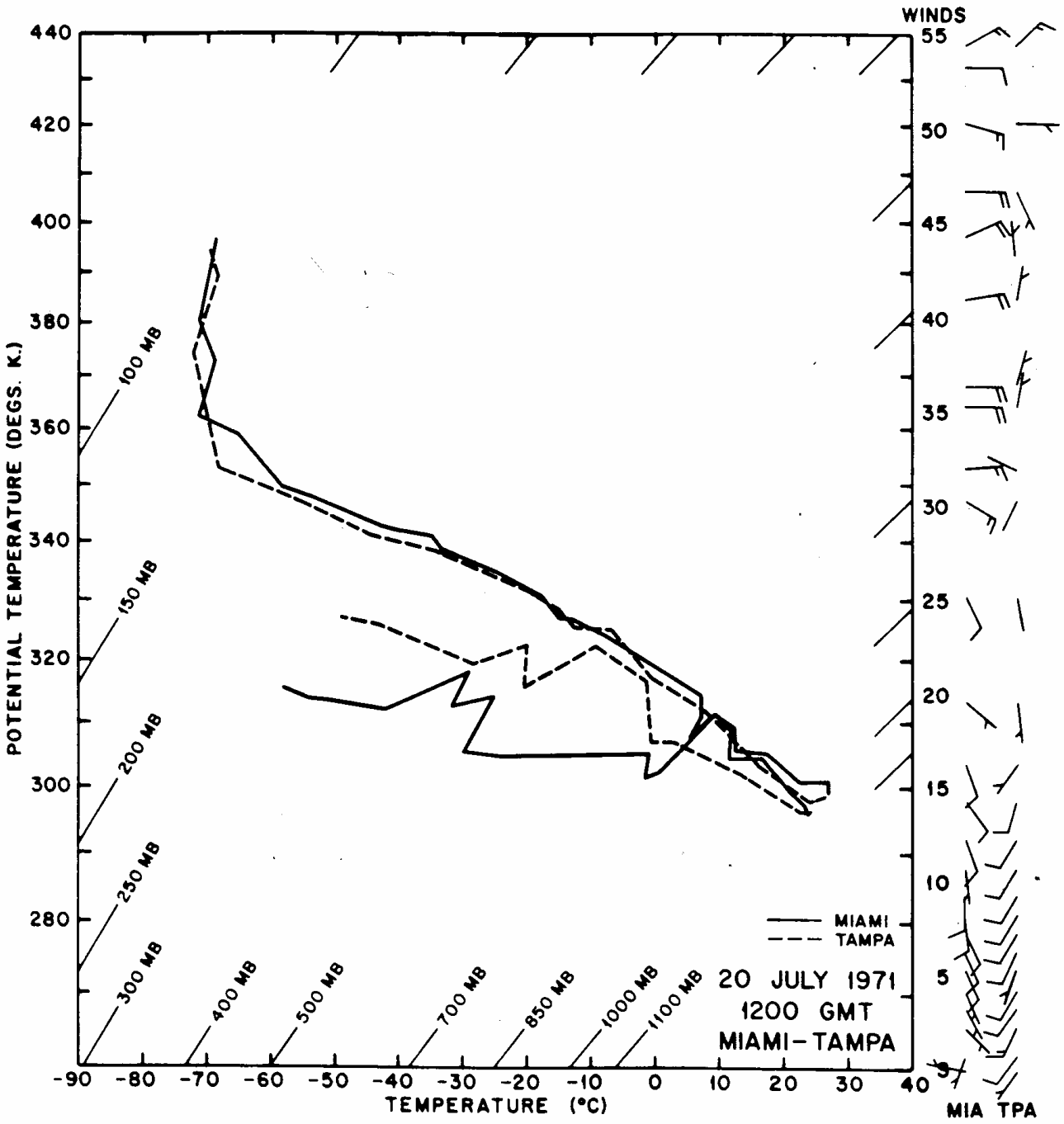

Figure 51. The radiosonde soundings at Miami and Tampa at 0700 EST on July 20, 1971.

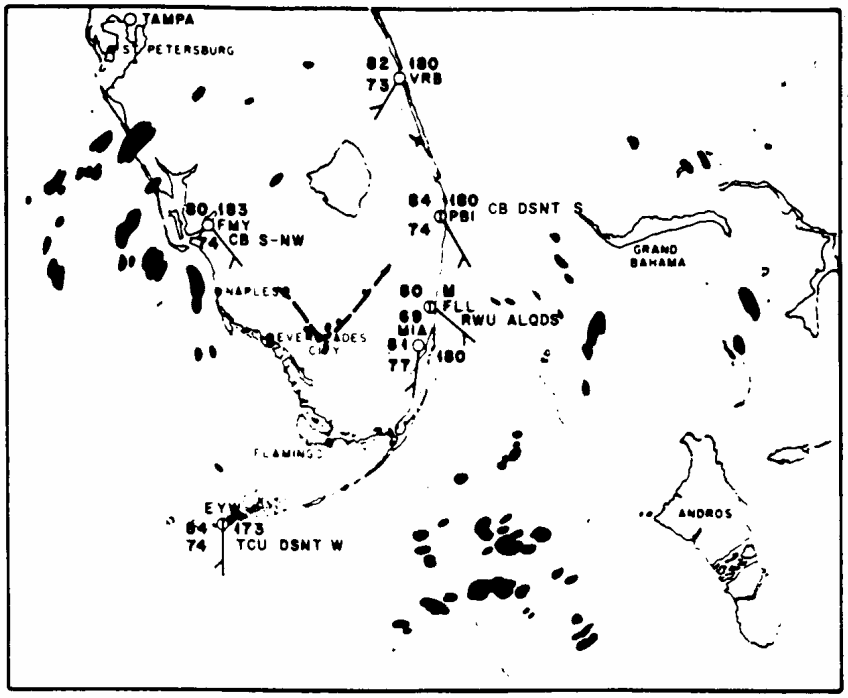

Figure 52. Miami WSR-57 radar echo coverage at 0759 EST and surface observations at 0800 EST on July 20, 1971.

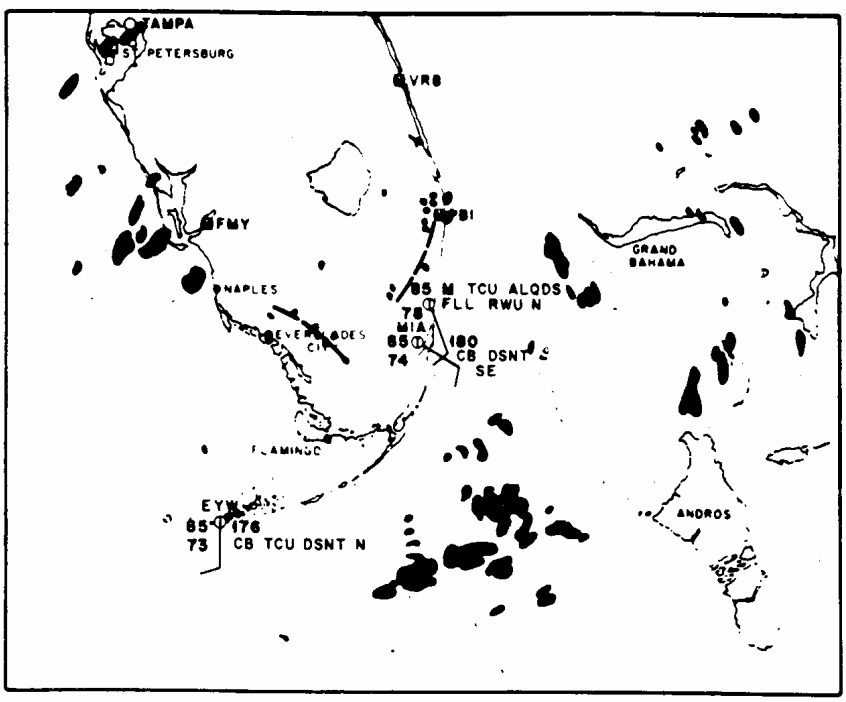

Figure 53. Miami WSR-57 radar echo coverage at 0901 EST and surface observations at 0900 EST on July 20, 1971.

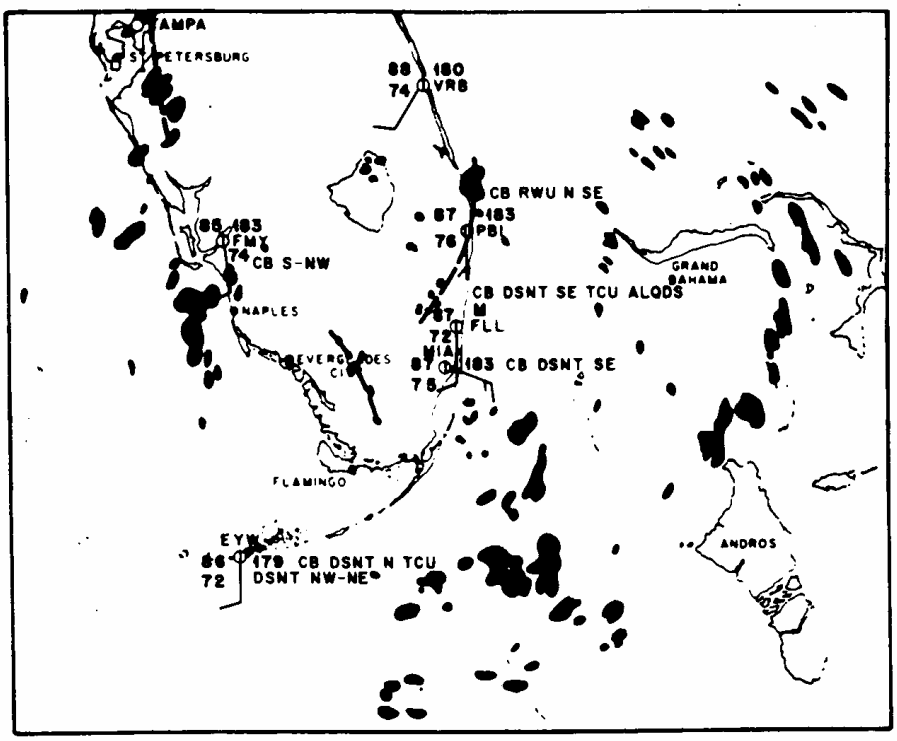

Figure 54. Miami WSR-57 radar echo coverage at 1002 EST and surface observations at 1000 EST on July 20, 1971.

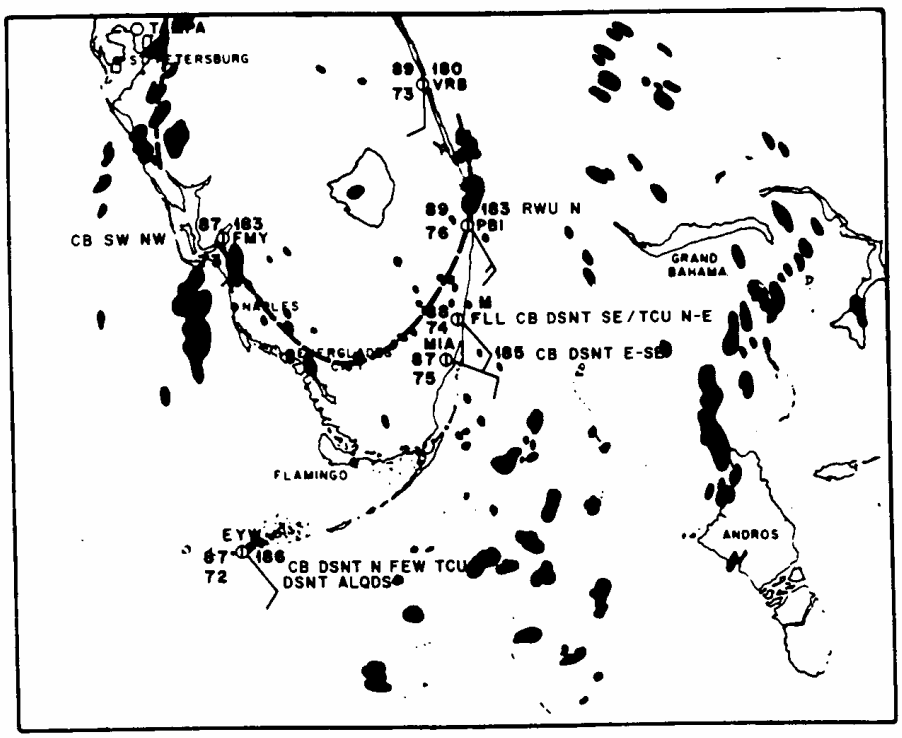

Figure 55. Miami WSR-57 radar echo coverage at 1059 EST and surface observations at 1100 EST on July 20, 1971.

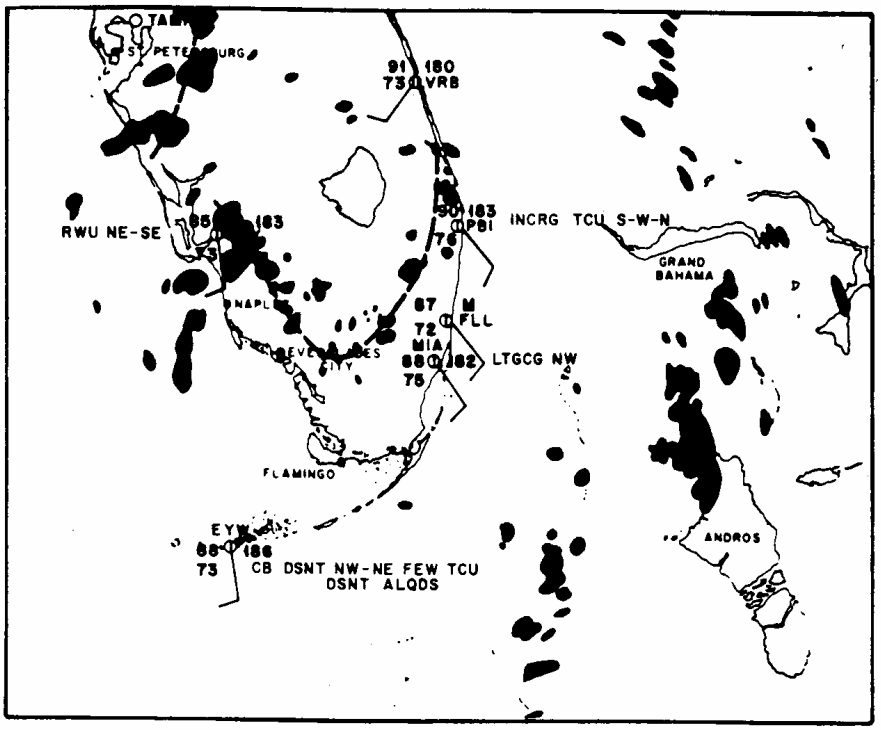

Figure 56. Miami WSR-57 radar echo coverage at 1203 EST and surface observations at 1200 EST on July 20, 1971.

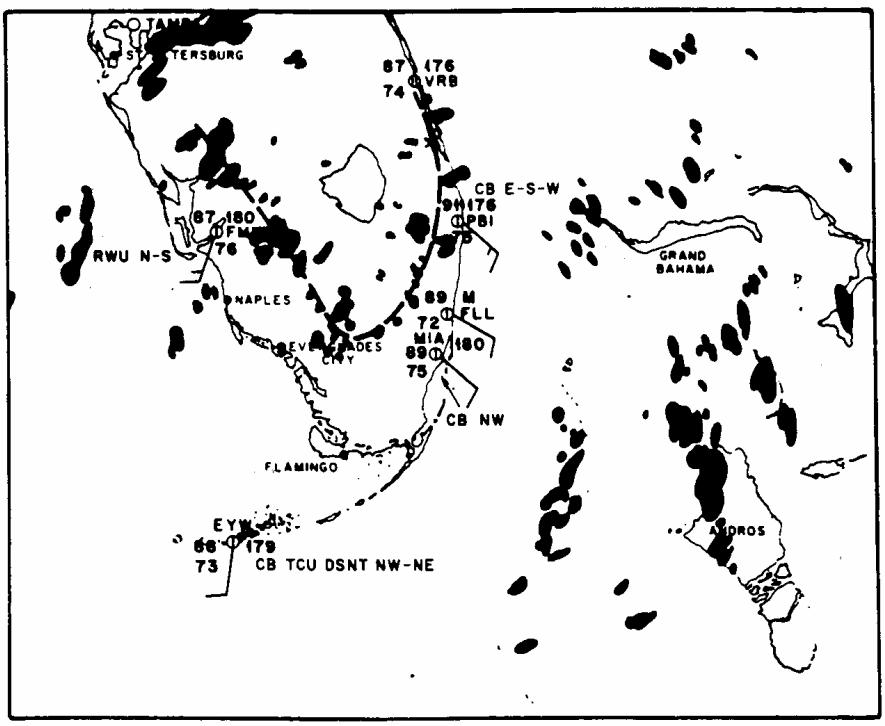

Figure 57. Miami WSR-57 radar echo coverage at 1302 EST and surface observations at 1300 EST on July 20, 1971.

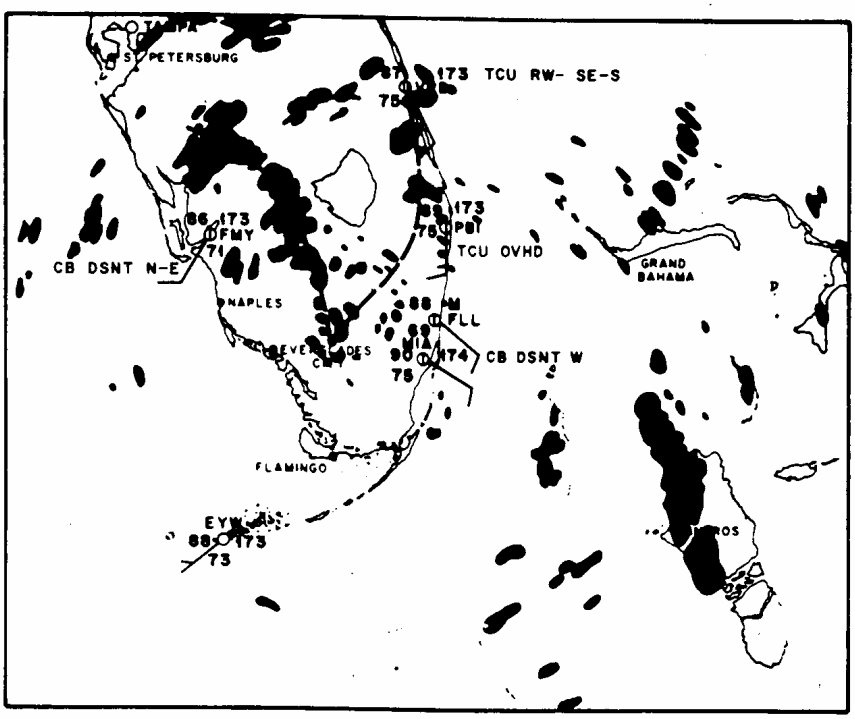

Figure 58. Miami WSR-57 radar echo coverage at 1359 EST and surface observations at 1400 EST on July 20, 1971.

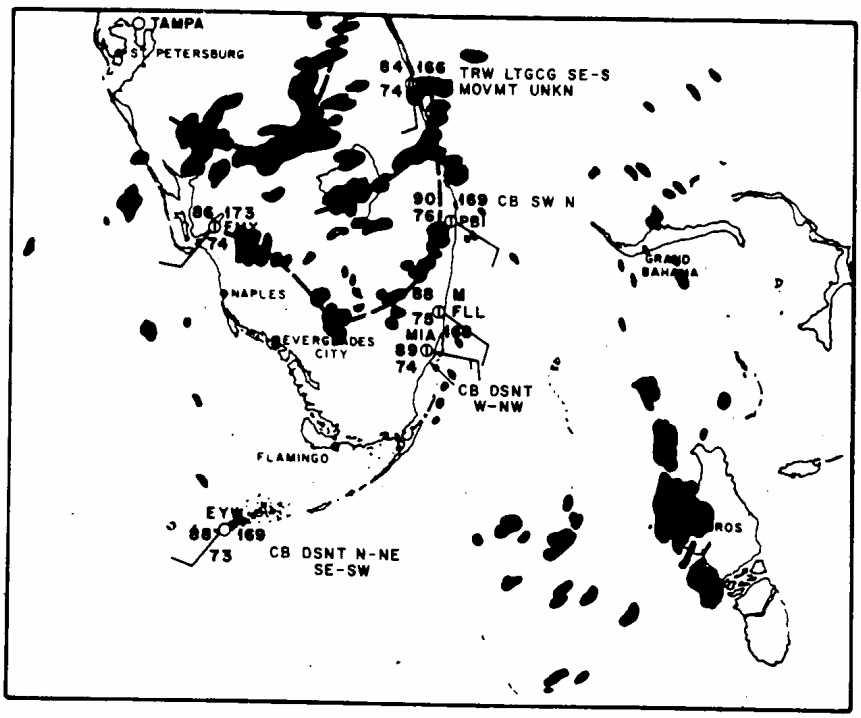

Figure 59. Miami WSR-57 radar echo coverage at 1459 EST and surface observations at 1500 EST on July 20, 1971.

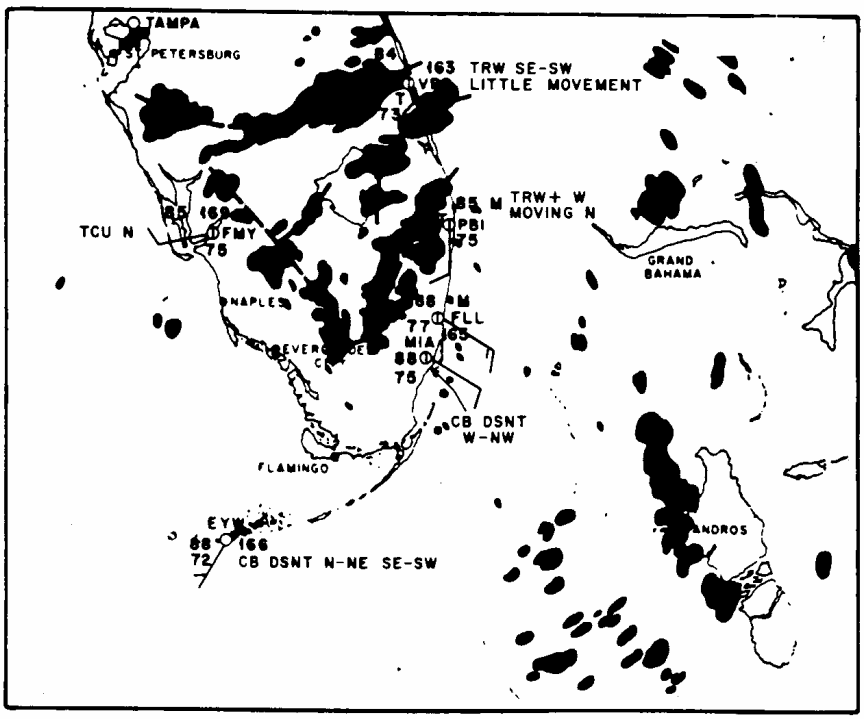

Figure 60. Miami WSR-57 radar echo coverage at 1605 EST and surface observations at 1600 EST on July 20, 1971.

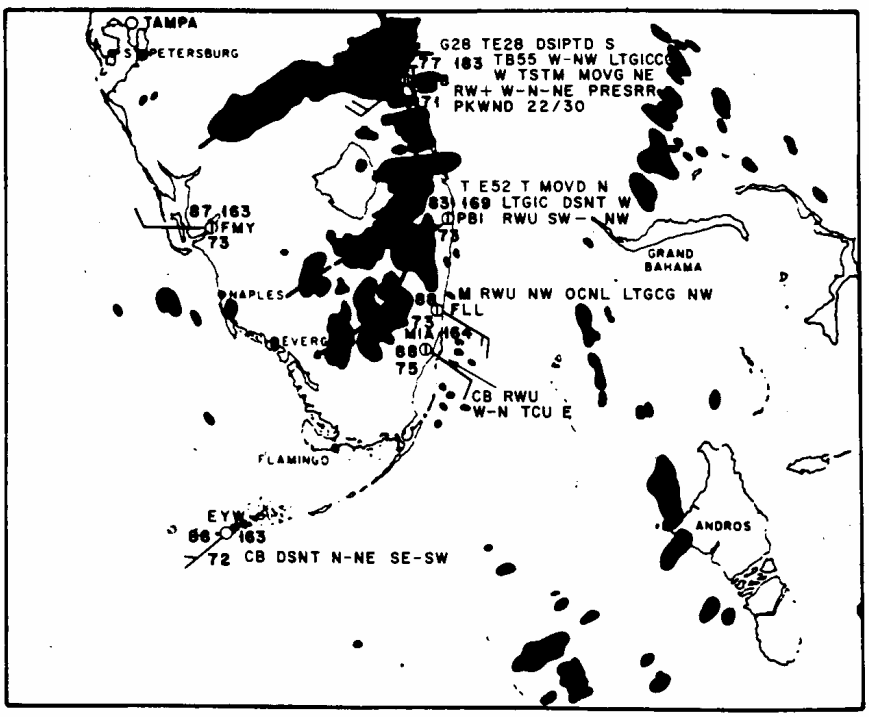

Figure 61. Miami WSR-57 radar echo coverage at 1657 EST and surface observations at 1700 EST on July 20, 1971.

Southwest wind case

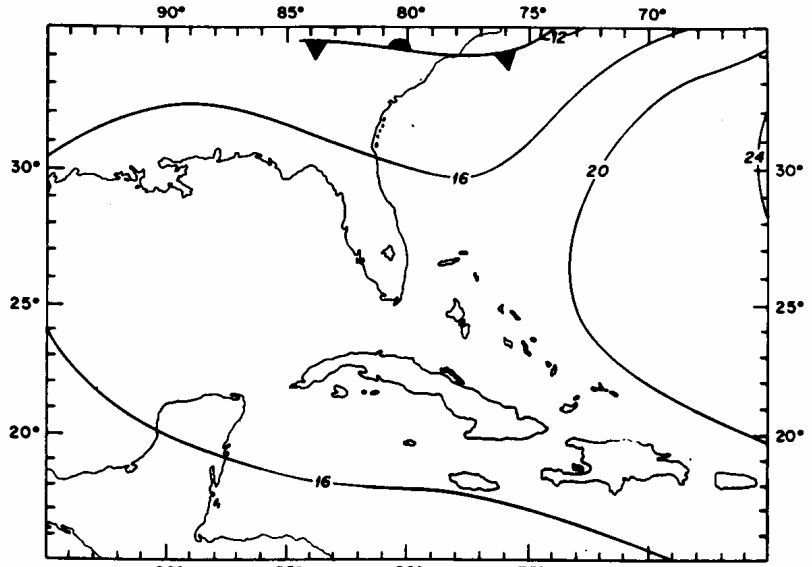

Figure 75. The surface analysis at 0700 EST on June 24, 1971.

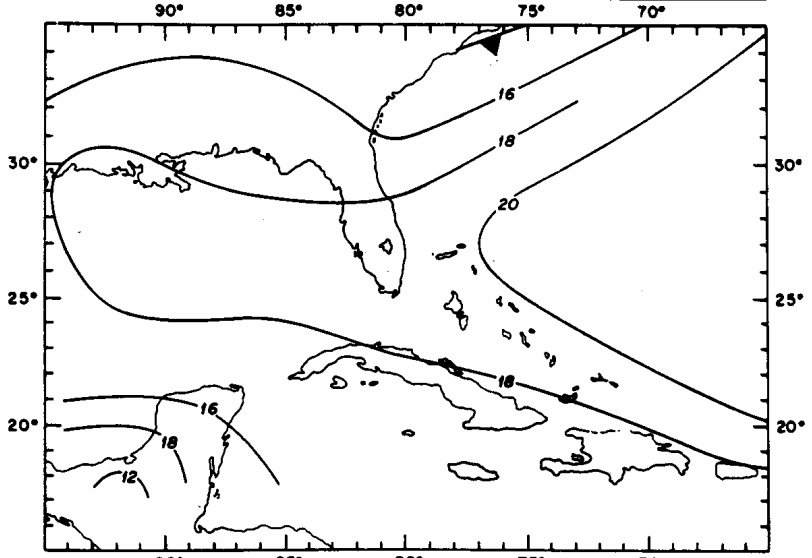

Figure 76. The surface analysis at 1300 EST on June 24, 1971.

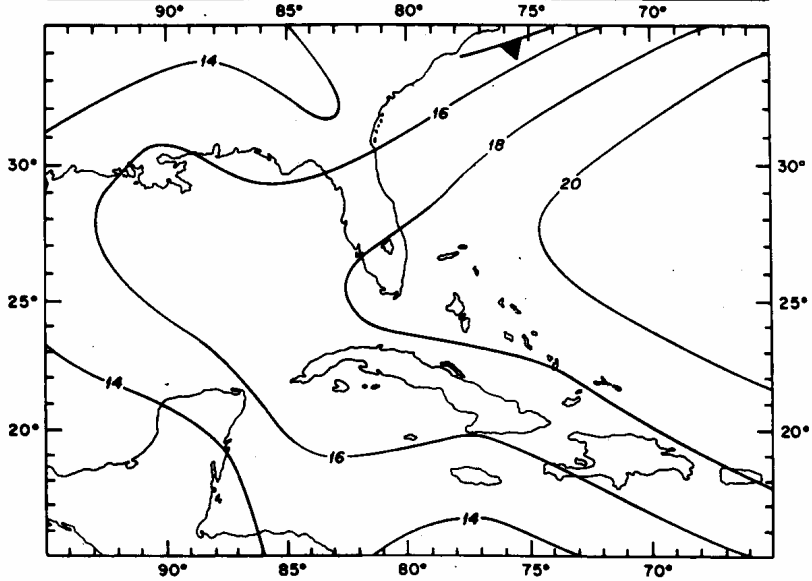

Figure 77. The surface analysis at 1900 EST on June 24, 1971.

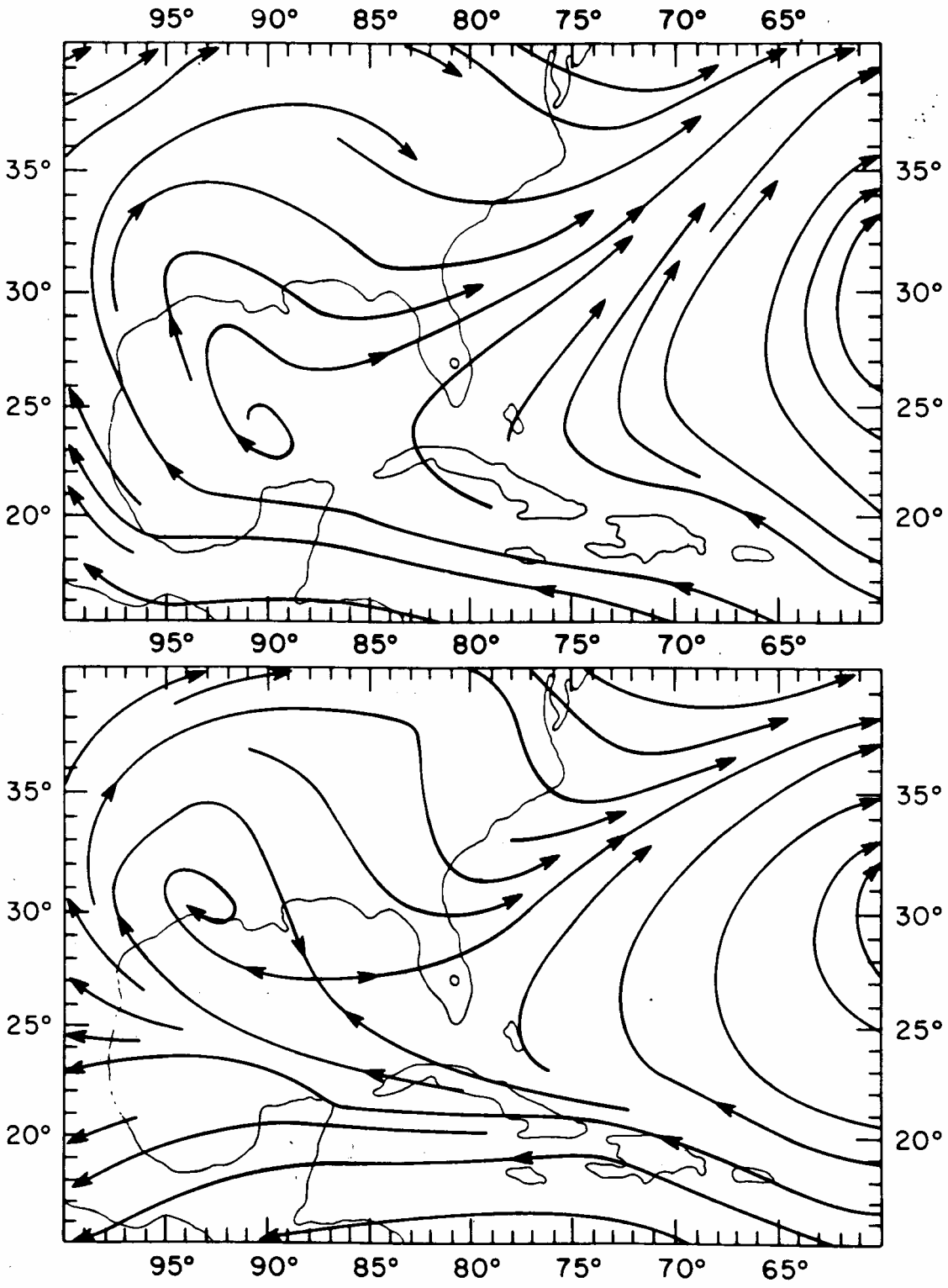

Figure 78. (top) Lower troposphere mean circulation 1000-600 mb layer at 0700 EST on June 24, 1971.

Figure 79. (bottom) Lower troposphere mean circulation 1000-600 mb layer at 1900 EST on June 24, 1971.

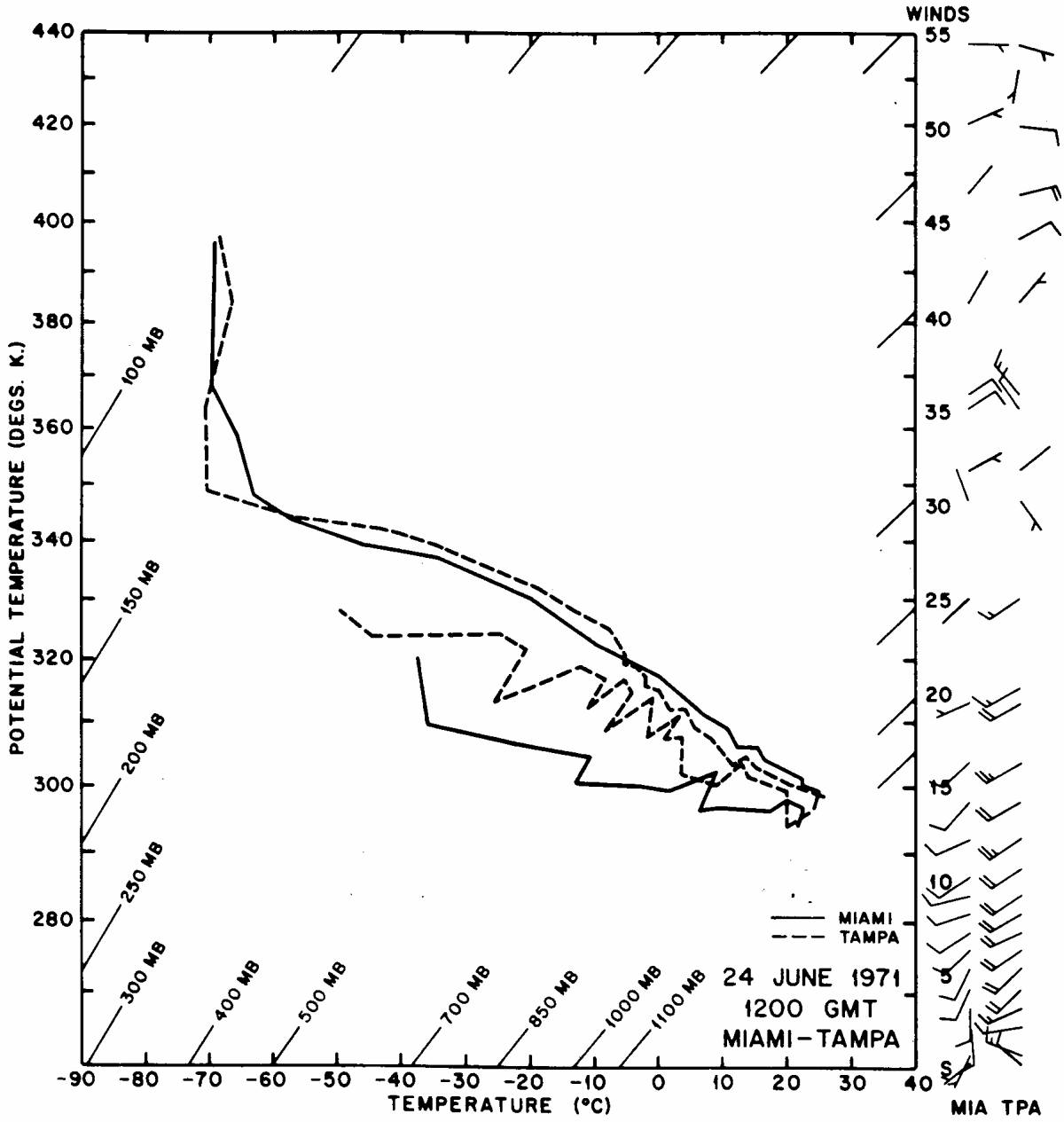

Figure 80. The radiosonde soundings at Miami and Tampa at 0700 EST on June 24, 1971.

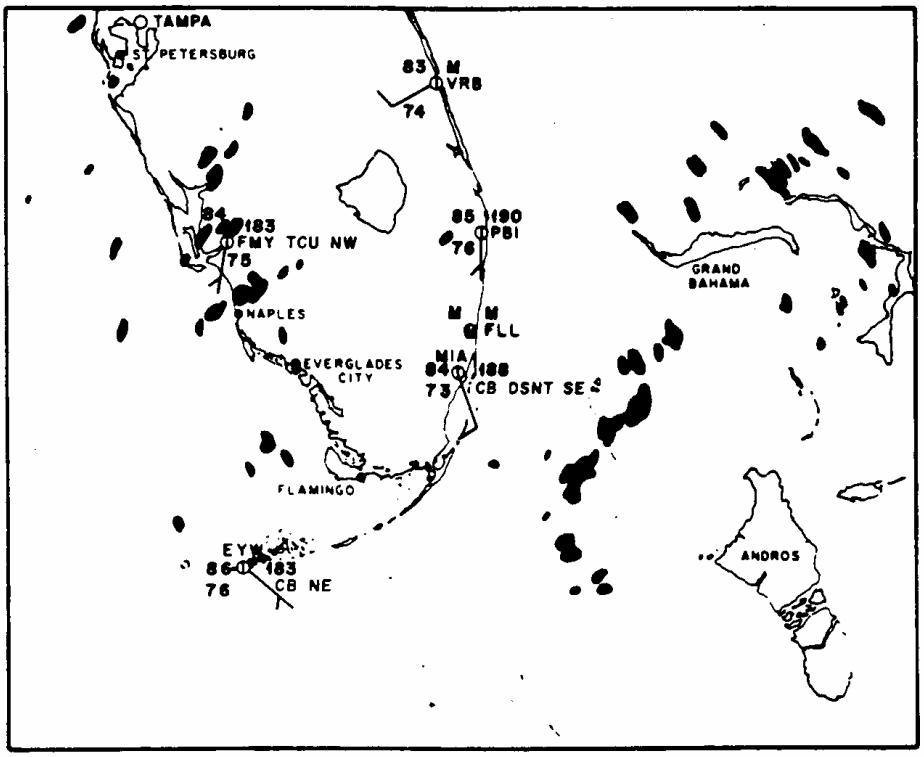

Figure 81. Miami WSR-57 radar echo coverage at 0858 EST and surface observations at 0900 EST on June 24, 1971.

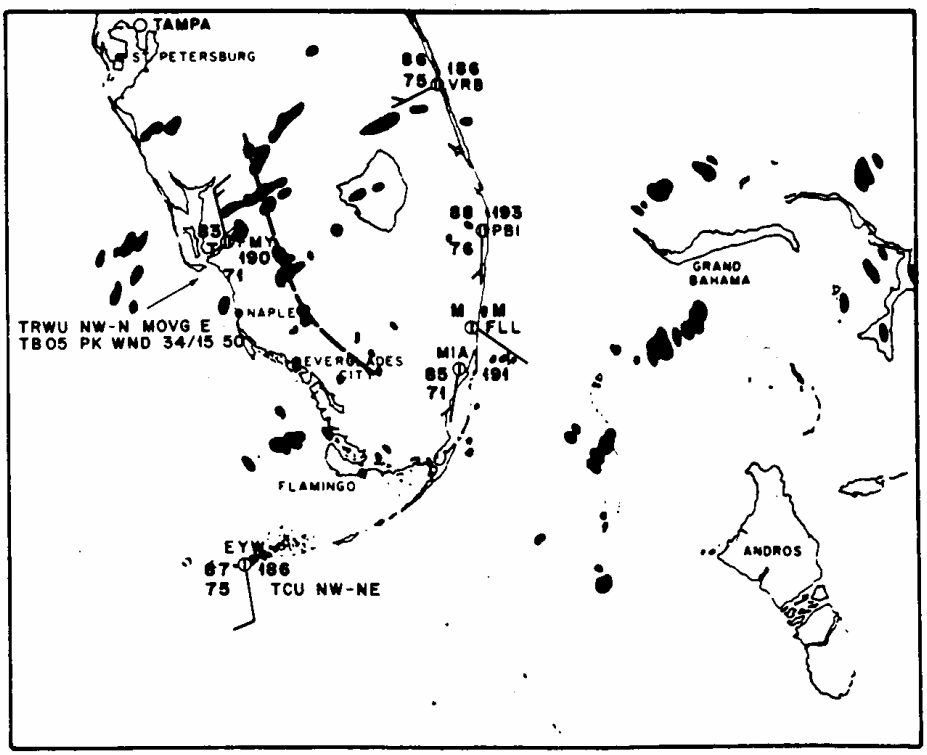

Figure 82. Miami WSR-57 radar echo coverage at 1003 EST and surface observations at 1000 EST on June 24, 1971.

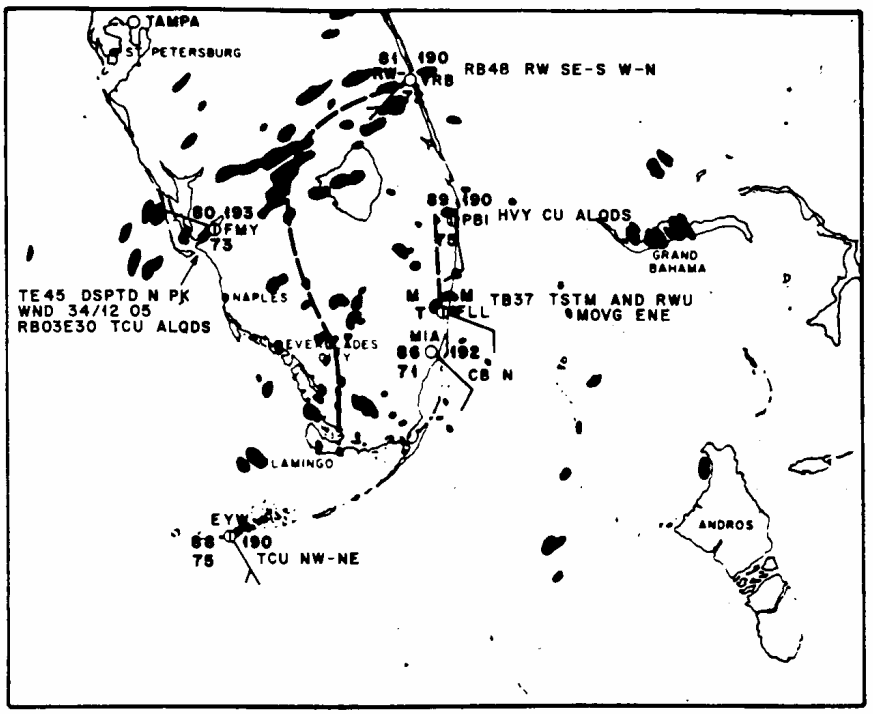

Figure 83. Miami WSR-57 radar echo coverage at 1103 EST and surface observations at 1100 EST on June 24, 1971.

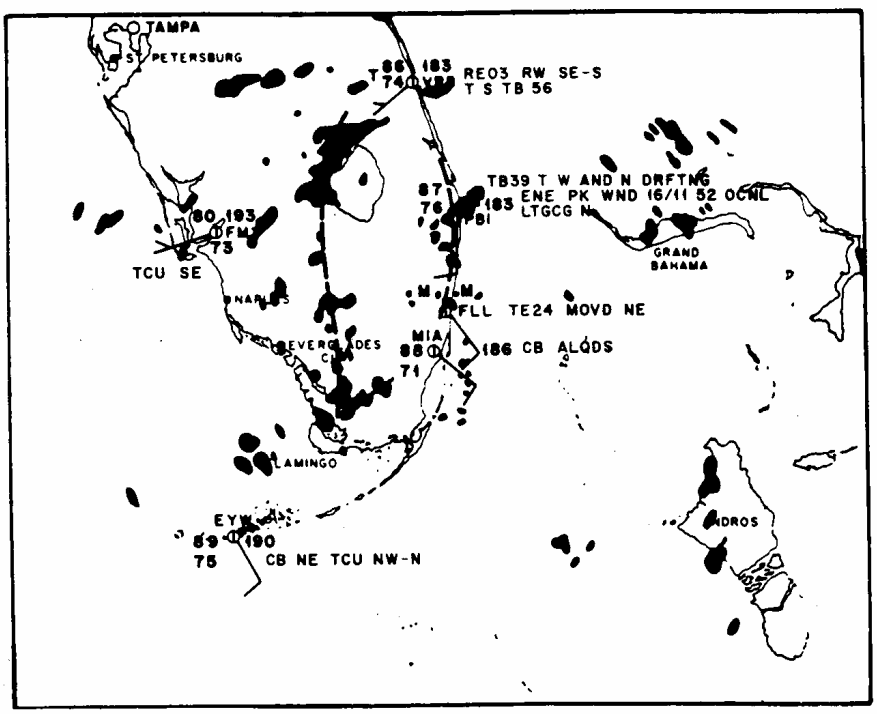

Figure 84. Miami WSR-57 radar echo coverage at 1203 EST and surface observations at 1200 EST on June 24, 1971.

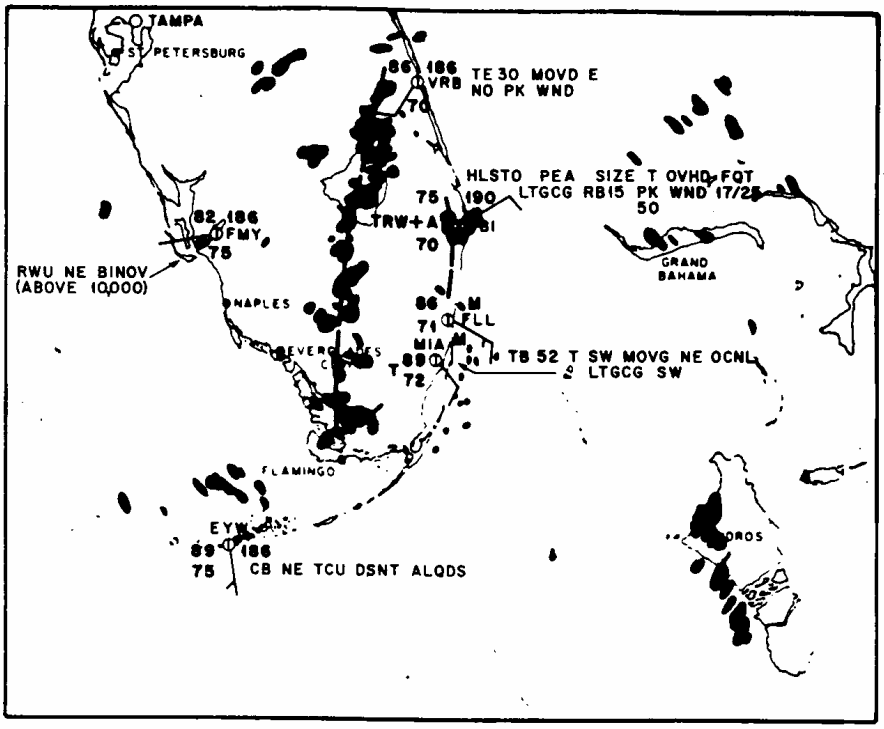

Figure 85. Miami WSR-57 radar echo coverage at 1248 EST and surface observations at 1300 EST on June 24, 1971.

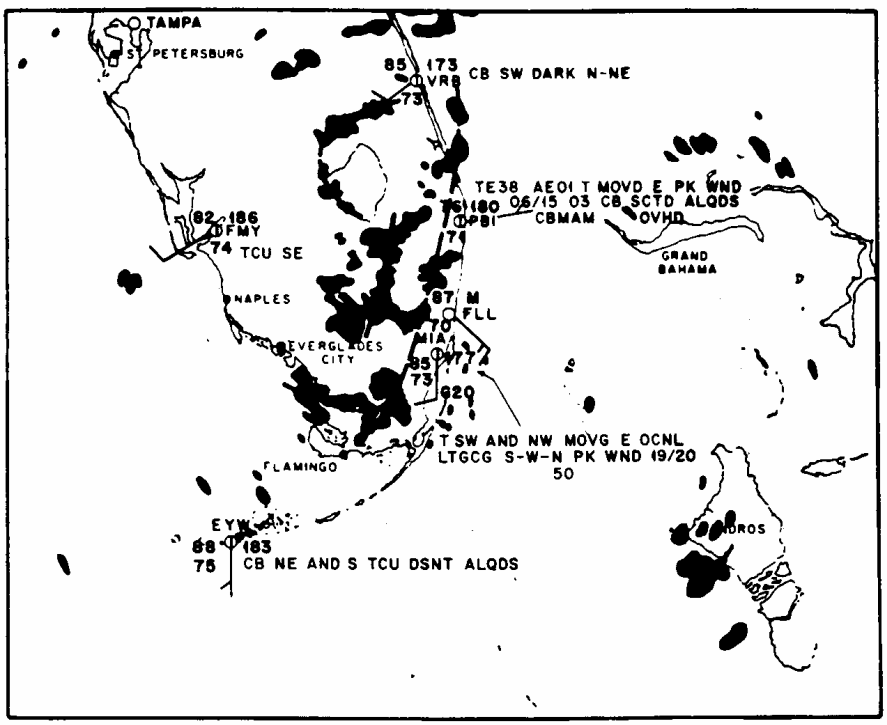

Figure 86. Miami WSR-57 radar echo coverage at 1359 EST and surface observations at 1400 EST on June 24, 1971.

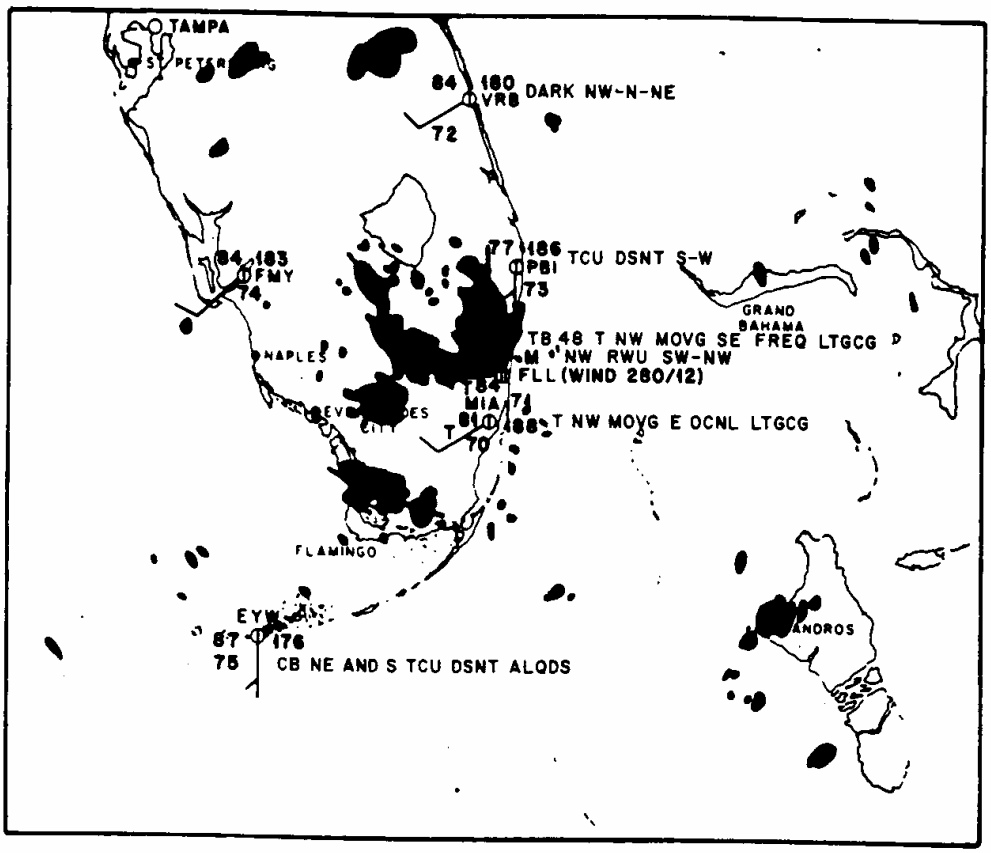

Figure 87. Miami WSR-57 radar echo coverage at 1458 EST and surface observations at 1500 EST on June 24, 1971.

Spatial Patterns of Convection in South Florida

David O. Blanchard and Raul E. Lopez

Monthly Weather Review, **113**, 1282-1299

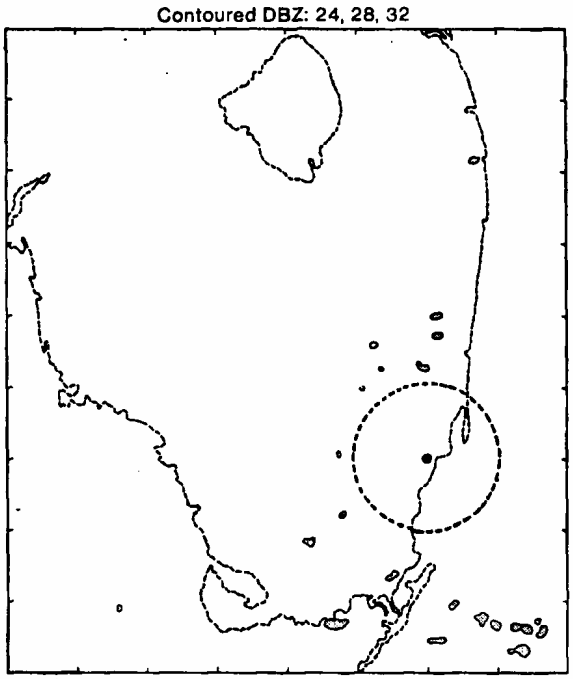

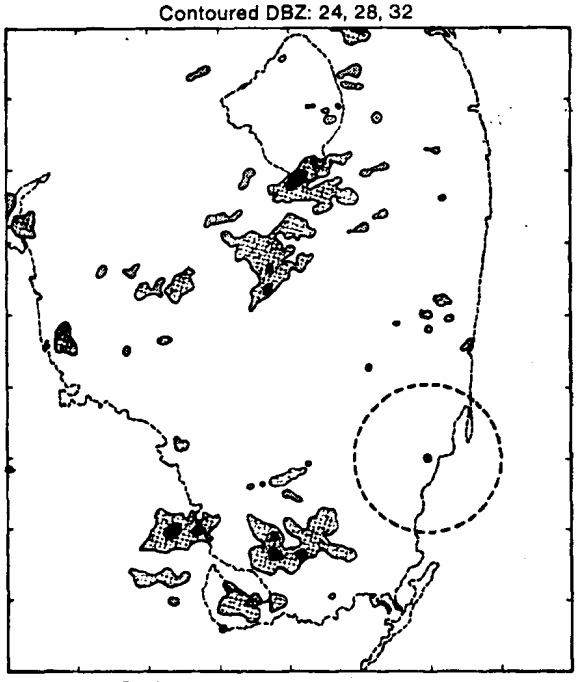

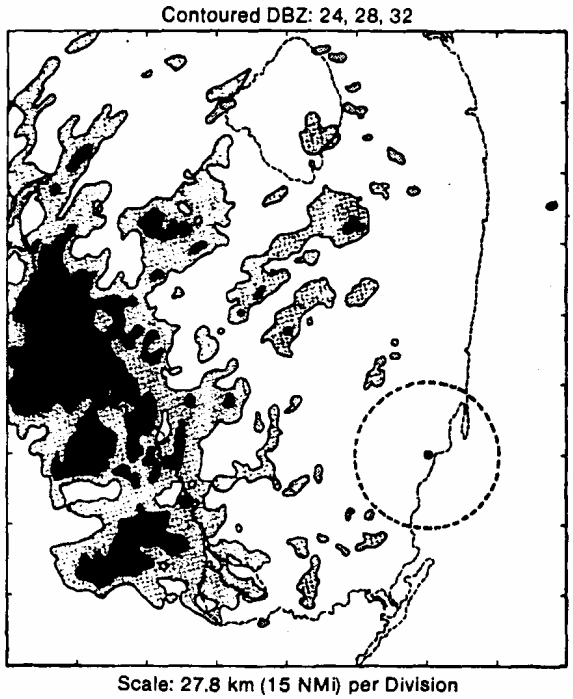

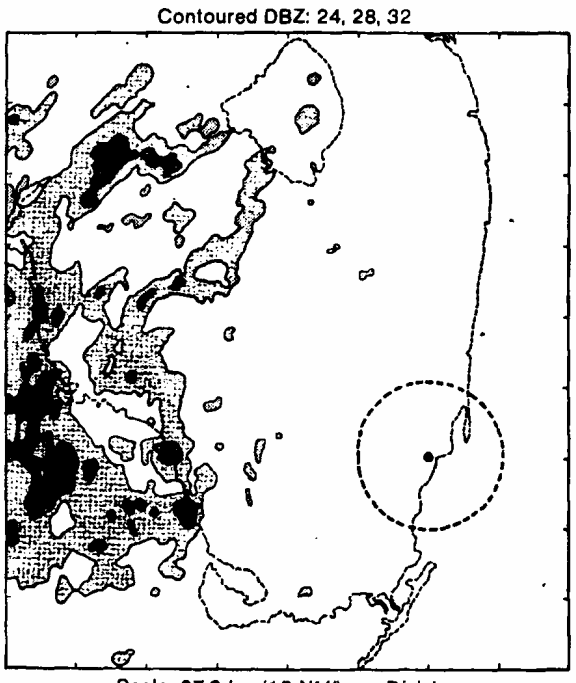

FIG. 3. As in Fig. 2 but for Type 2 days.

(a)

(b)

FIG. 12. As in Fig. 11 but for Type 2 days.

Type 2 Days:

Convection starts along the east coast, is quickly advected to the west coast where the two sea-breeze convergence zones merge, producing strong convection which is modified by the curvature of the coastline, and is finally advected out to sea. Synoptically the western extension of the Atlantic subtropical high is absent and a high-pressure system located over the southeastern US extends its influence over the Florida peninsula. Owing to the extreme subsidence associated with the high pressure system, convection is sparse. Only when the east coast sea-breeze merges with the west coast sea-breeze (this occurs easily as the synoptic-scale wind is stronger than average), is convergence strong enough to generate convection.

Type 4 Days:

They comprise many types of disturbed days including tropical disturbances (easterly waves, tropical depressions, etc), westerly disturbances (middle latitude short waves, dissipating cold fronts), upper tropospheric lows, and very moist tropical air. The behavior of the convection is unique to the particular nature of the disturbance, but rainfall is generally strong and widespread. Often within the widespread pattern of convection and rainfall, Type 1, 2, or 3 patterns of convective rainfall can be discerned as being embedded within the system. Generally disturbed convection is weak (vertical velocities, not rainfall), as the stability is nearly wet adiabatic, and this is not as conducive to anvil production, although widespread cirrus may be present due to large-scale lifting.

Cloud Microphysics of Florida Convection

CCN variability across the Florida Peninsula

Sax, R.I. and James G.Hudson, 1981: Continentality of the south Florida summertime CCN aerosol. *J. Atmos. Sci.*, **38**, 1467-1479.

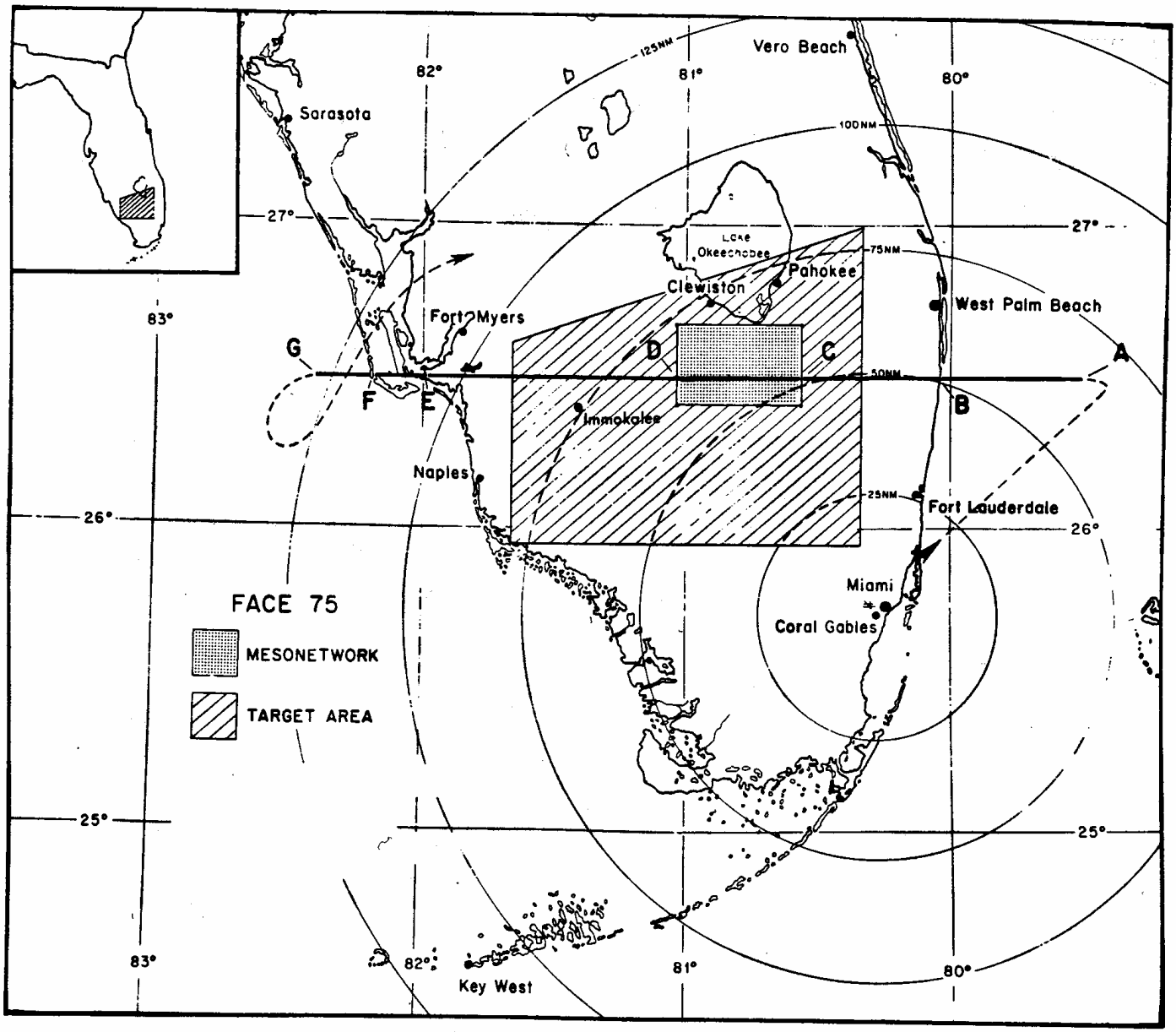

FIG. 1. FACE target area with DC-6 flight track for cloud-base CCN study (FACE 75) superimposed.

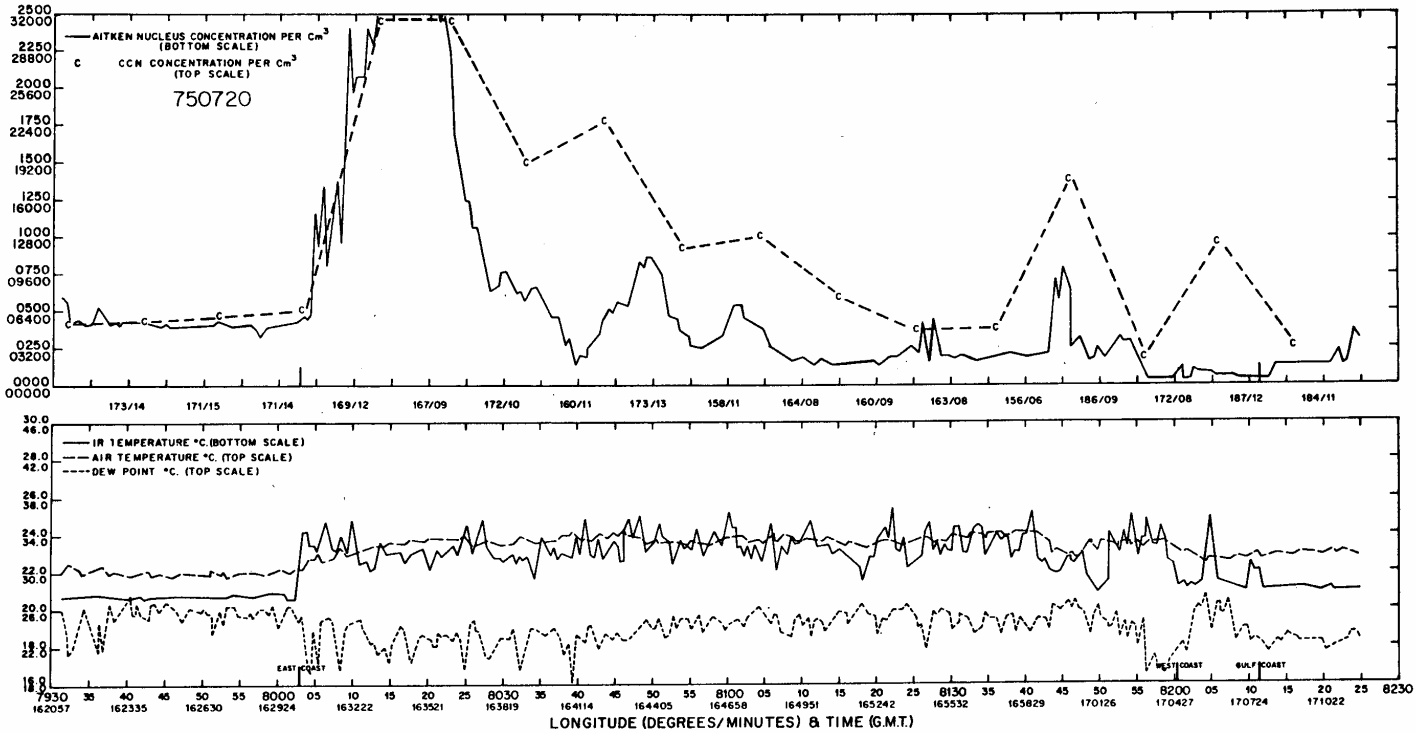

FIG. 2. Cross-peninsula profile of aerosol and meteorological data acquired at the cloud base level on 20 July 1975.

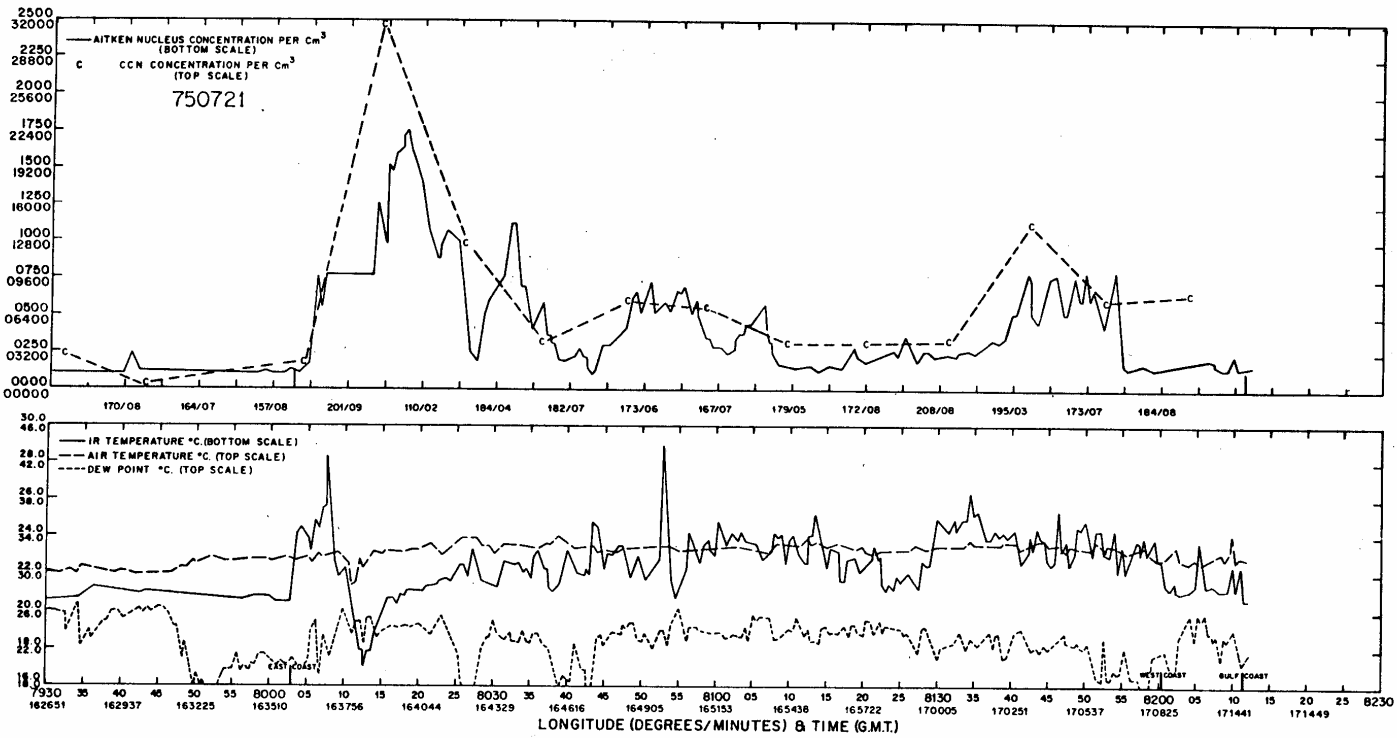

FIG. 3. As in Fig. 2 except on 21 July 1975.

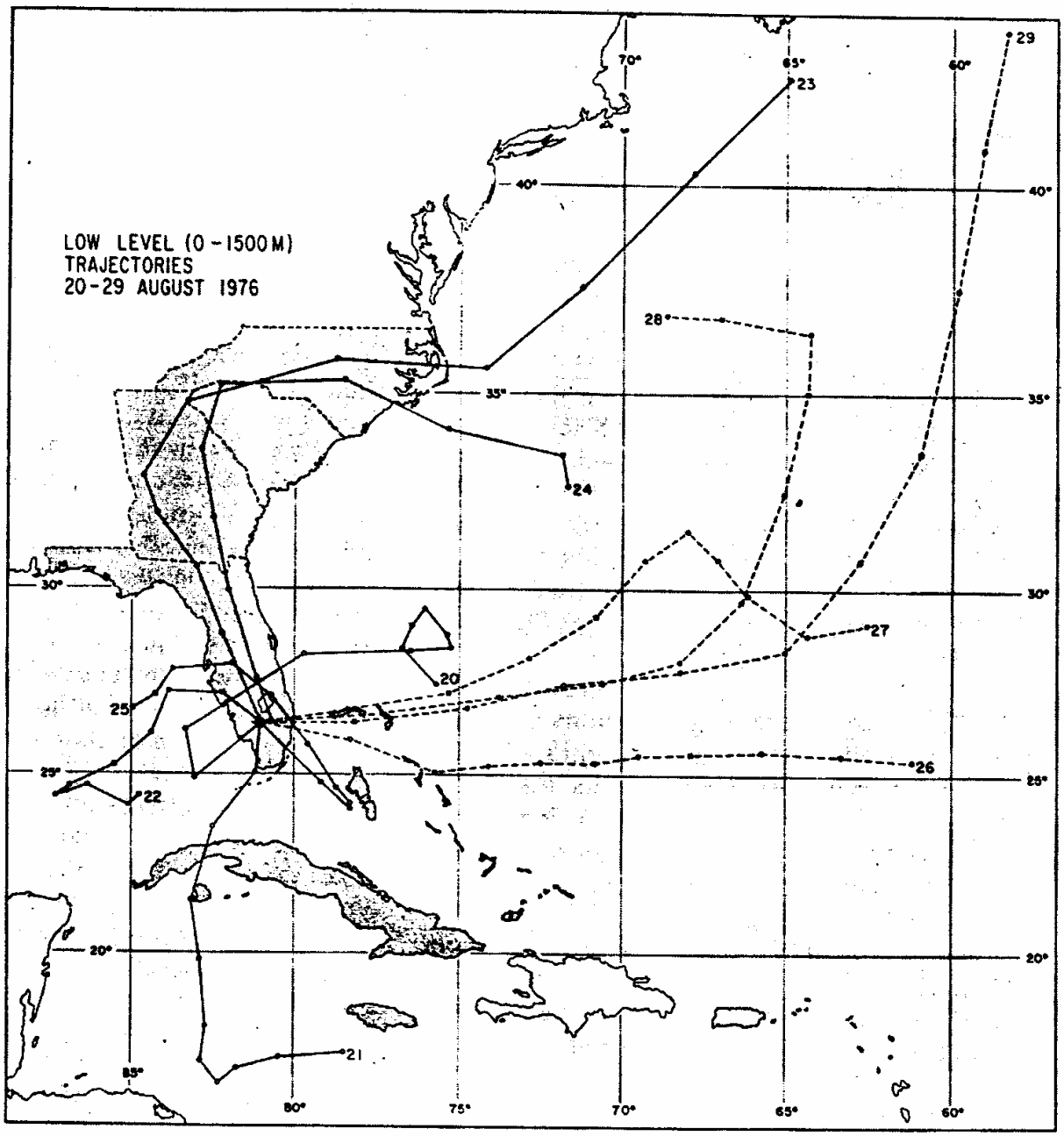

FIG. 7. Low-level air mass trajectories (5-day) terminating in the center of the FACE target area at 1800 GMT on each of 10 days during the period 20–29 August 1976.

Summary

- CCN concentrations are extremely variable across the Florida Peninsula. At 0.75% supersaturation concentrations range from 250 to 2500 cm^{-3}.
- Possible local sources of CCN are anthropogenic in Miami area, biological decay over peat and muck fields and over Everglades provide copious sources of ammonia that combines with SO_2 to form ammonium sulfate particles.

Precipitation evolution in Florida Cumuli

Sources:

Willis, Paul T., and John Hallet, 1991: Microphysical measurements from an aircraft ascending with a growing isolated maritime cumulus tower. *J. Atmos. Sci*., **48**, 283-300.

Sax, Robert I., and Vernon W. Keller, 1980: Water-ice and water-updraft relationships near -10°C within populations of Florida cumuli. *J. Appl. Met.*, **19**, 505-514.

Keller, Vernon W., and Robert I. Sax, 1981: Microphysical development of a pulsating cumulus tower. *Quart. J.R. Met. Soc*., **107**, 679-697.

Hallett, John, Robert I. Sax, Dennis Lamb, and A.S. Ramachandra Murty, 1978: Aircraft measurements of ice in Florida cumuli. *Quart. J.R. Met. Soc. **104**, 631-651.*

- Strong evidence for warm-rain (collision and coalescence) in lower portions of clouds.
- Graupel forms rapidly in cumulus clouds.
- Evolution of ice and water are consistent with a rime-splintering, secondary ice production process.
- The presence of supercooled raindrops accelerates the rate of production of graupel particles and dominance of the ice phase.

Speculations on Anvil Dynamics

We want to measure the efficiency of convective moisture transport into anvils. We define "Anvil efficiency" (AE) as

$$AE = \frac{upper\ troposphere\ moisture\ divergence}{CB\ sub\text{–}cloud\text{–}base\ moisture\ convergence}$$

I speculate that AE is much lower in transient cells with moving convergence lines than in persistent cells along "merged" sea breeze convergence lines.

Speculations cont.

I define another parameter, tropopause transport efficiency (TTE) as:

$$TTE = \frac{moisture\ flux\ across\ the\ tropopause}{CB\ \ sub\text{–}cloud\text{–}base\ moisture\ convergence}$$

TTE should be higher in cells along merged convergence lines.

Both AE and TTE should vary inversely with PE. CB's with lower CCN and high GCCN concentrations, should exhibit high PE's and hence lower AE's and TTE's.

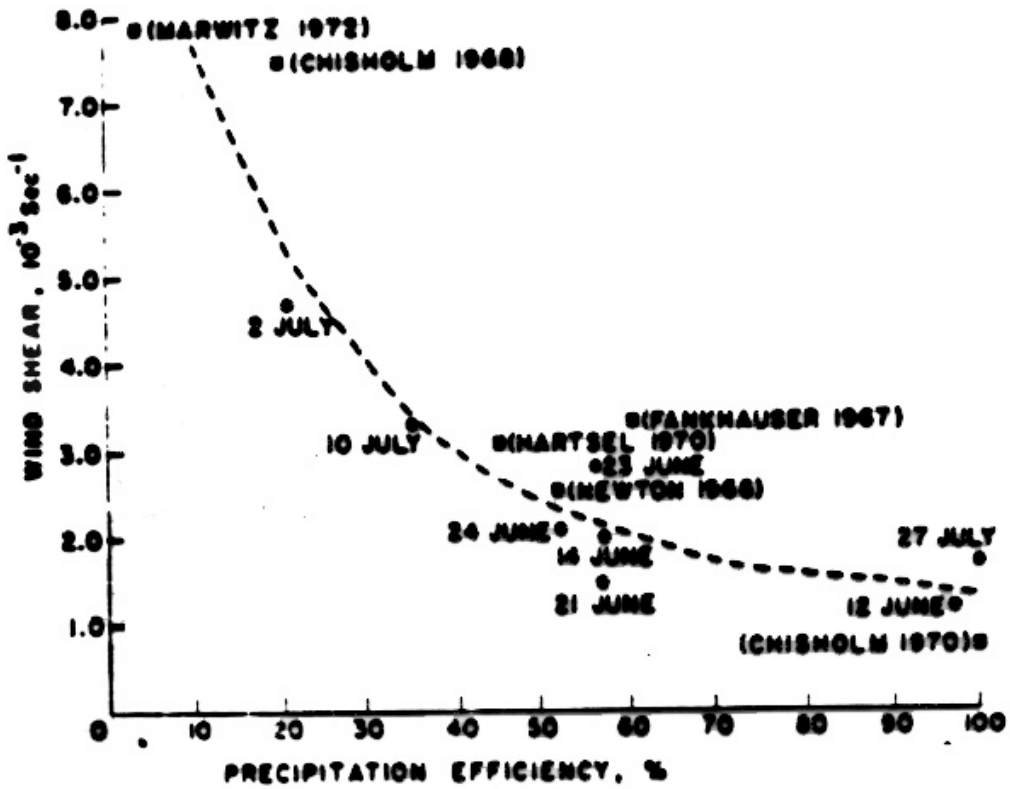

However, Braham (1952) estimated PE in Florida and Ohio Cb's to be only 10% even though wind shears were weak.

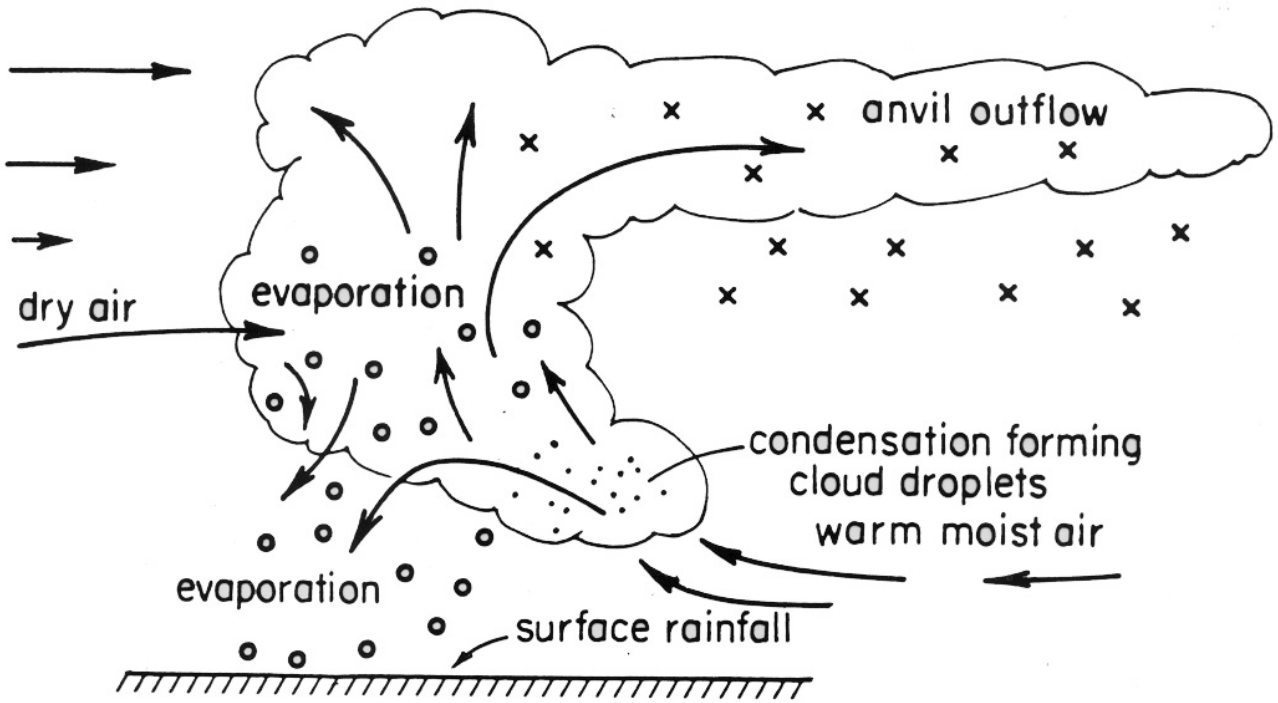

Newton (1966) estimated in a squall line Cb that 45-50% of moisture entering cloud base reaches the ground, 40% evaporates as downdrafts, and 10% is injected into anvils.

El Niño and LaNiña

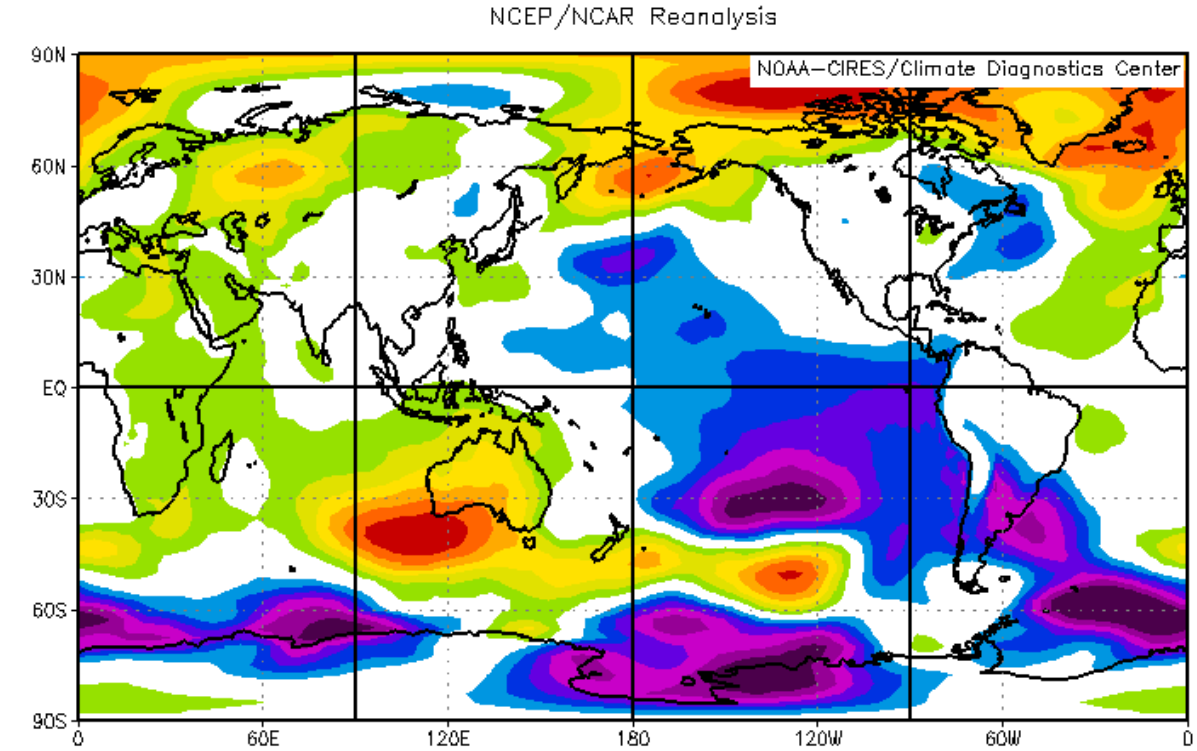
NCEP/NCAR Reanalysis
NOAA–CIRES/Climate Diagnostics Center
90N
60N
30N
EQ
30S
60S
90S
0
60E
120E
180
120W
60W
0
Surface Pressure (mb) Composite Anomaly
ul : 1951,1953,1957,1963,1965,1972,1977,1982,1993,1997 minus 1950,1954,1955,1956,1964,1970,1971,1975,1
−3
−2
−1
0
1
2
3

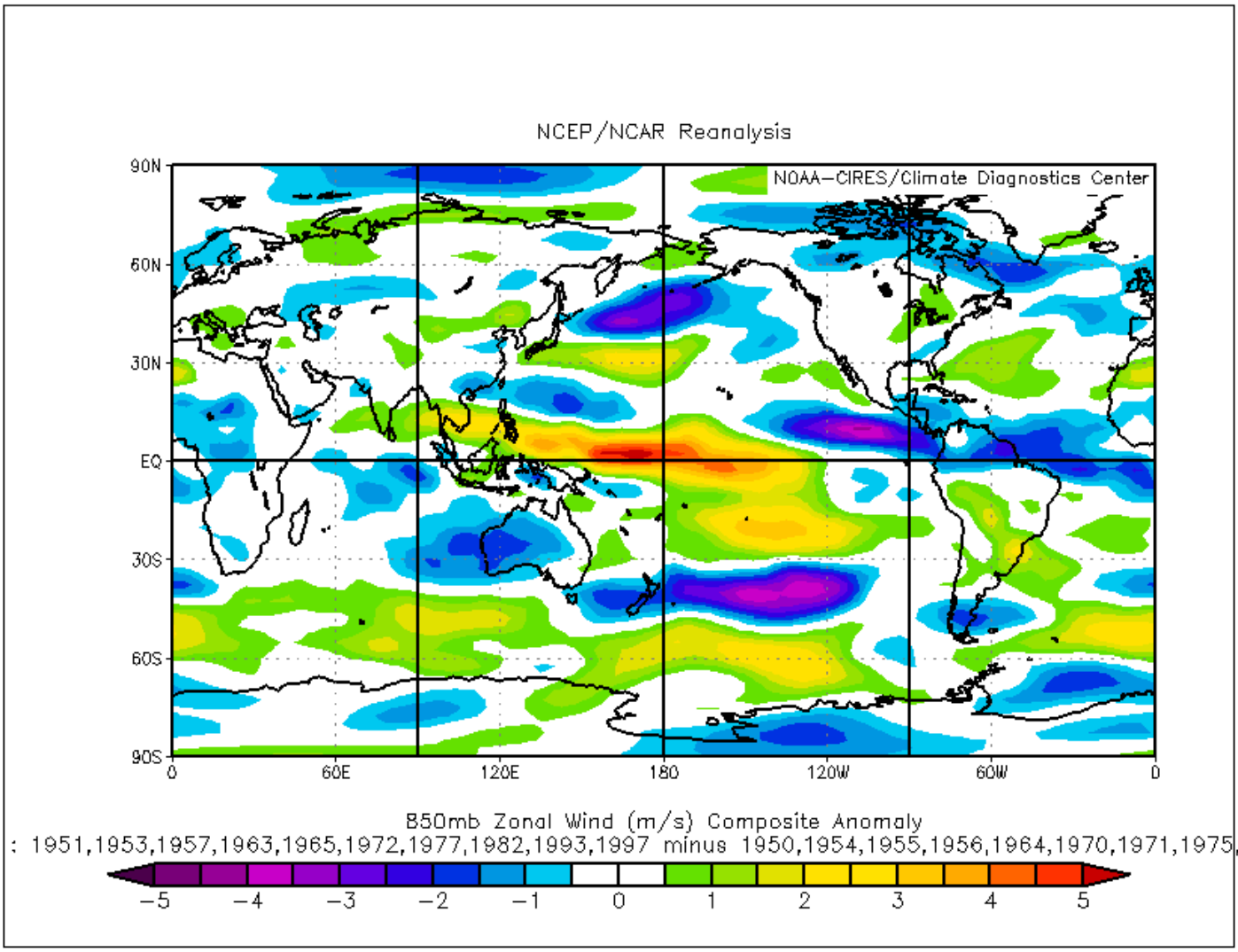
NCEP/NCAR Reanalysis
NOAA–CIRES/Climate Diagnostics Center
90N
60N
30N
EQ
30S
60S
90S
0
60E
120E
180
120W
60W
0
850mb Zonal Wind (m/s) Composite Anomaly
ul : 1951,1953,1957,1963,1965,1972,1977,1982,1993,1997 minus 1950,1954,1955,1956,1964,1970,1971,1975,1
−5
−4
−3
−2
−1
0
1
2
3
4
5

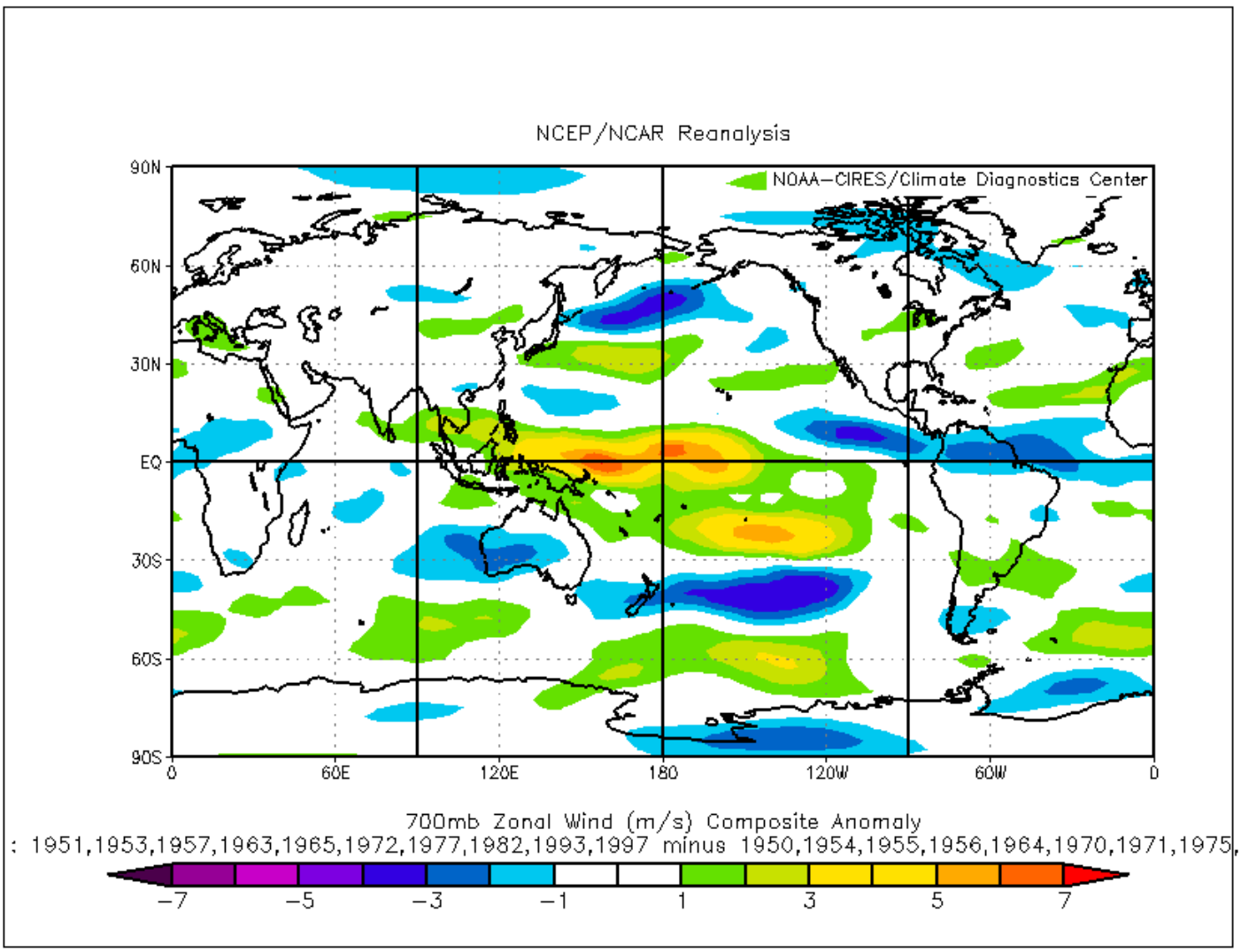
NCEP/NCAR Reanalysis
NOAA–CIRES/Climate Diagnostics Center
90N
60N
30N
EQ
30S
60S
90S
0
60E
120E
180
120W
60W
0
700mb Zonal Wind (m/s) Composite Anomaly
ul : 1951,1953,1957,1963,1965,1972,1977,1982,1993,1997 minus 1950,1954,1955,1956,1964,1970,1971,1975,1
−7
−5
−3
−1
1
3
5
7

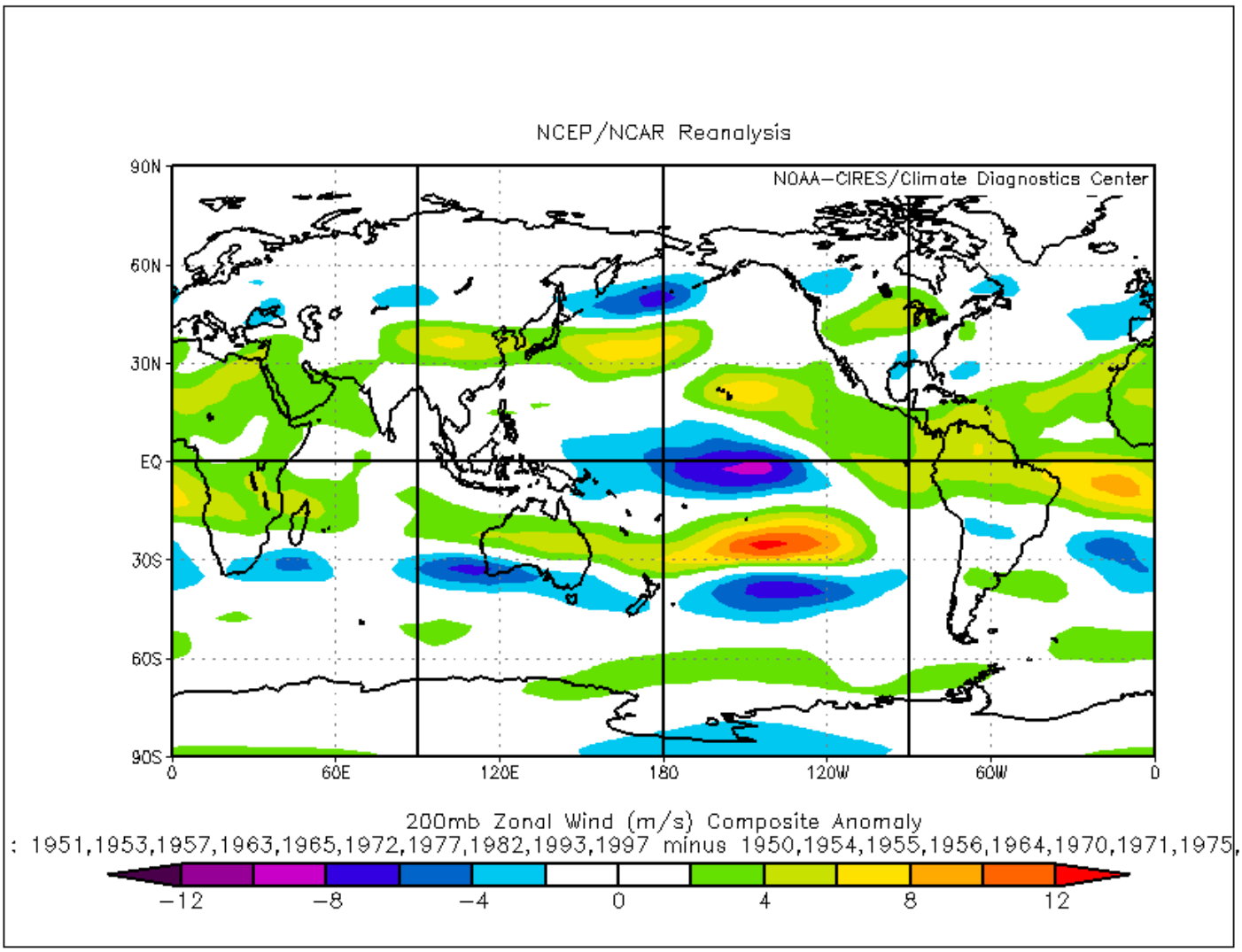
NCEP/NCAR Reanalysis
NOAA–CIRES/Climate Diagnostics Center
90N
60N
30N
EQ
30S
60S
90S
0
60E
120E
180
120W
60W
0
200mb Zonal Wind (m/s) Composite Anomaly
ul : 1951,1953,1957,1963,1965,1972,1977,1982,1993,1997 minus 1950,1954,1955,1956,1964,1970,1971,1975,1
−12
−8
−4
0
4
8
12

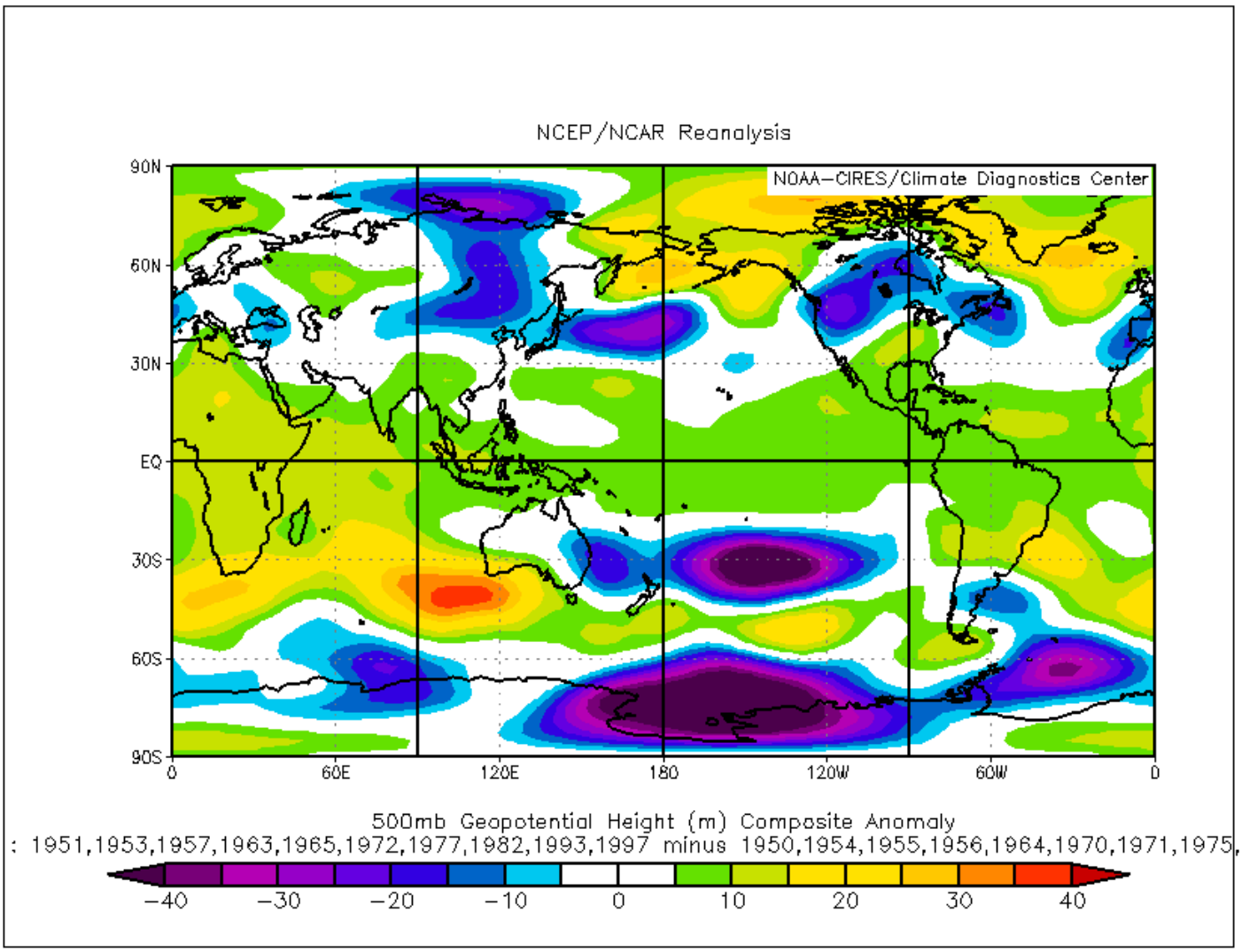
NCEP/NCAR Reanalysis
NOAA–CIRES/Climate Diagnostics Center
90N
60N
30N
EQ
30S
60S
90S
0
60E
120E
180
120W
60W
0
500mb Geopotential Height (m) Composite Anomaly
ul : 1951,1953,1957,1963,1965,1972,1977,1982,1993,1997 minus 1950,1954,1955,1956,1964,1970,1971,1975,1
−40
−30
−20
−10
0
10
20
30
40

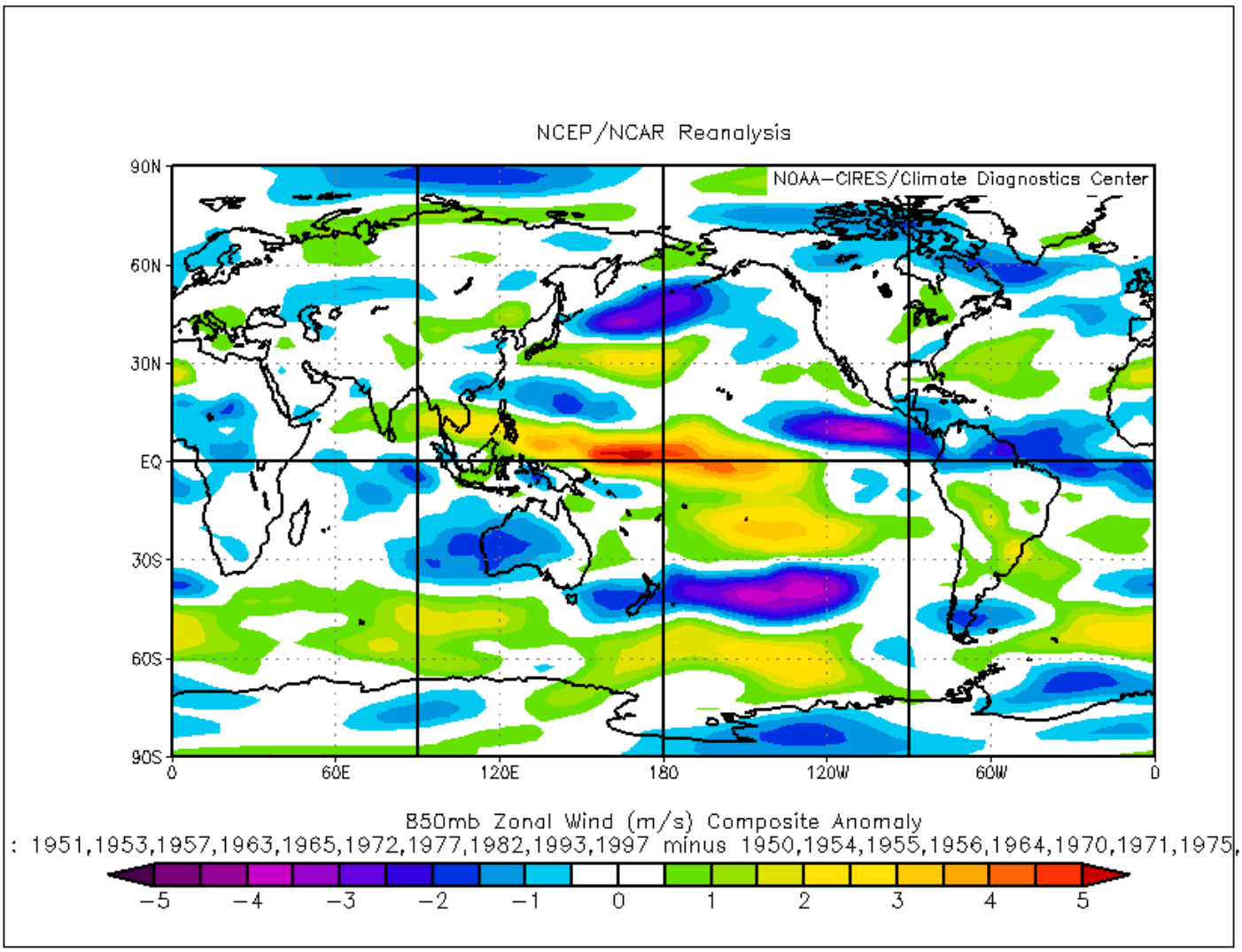
NCEP/NCAR Reanalysis
NOAA–CIRES/Climate Diagnostics Center
90N
60N
30N
EQ
30S
60S
90S
0
60E
120E
180
120W
60W
0
850mb Zonal Wind (m/s) Composite Anomaly
ul : 1951,1953,1957,1963,1965,1972,1977,1982,1993,1997 minus 1950,1954,1955,1956,1964,1970,1971,1975,1
−5
−4
−3
−2
−1
0
1
2
3
4
5

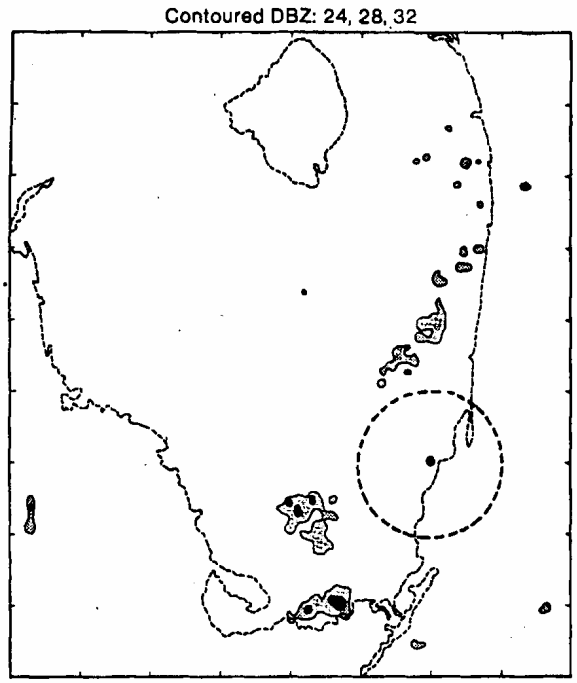

Scale: 27.8 km (15 NMi) per Division
from 900 to 1200 EDT

(a)

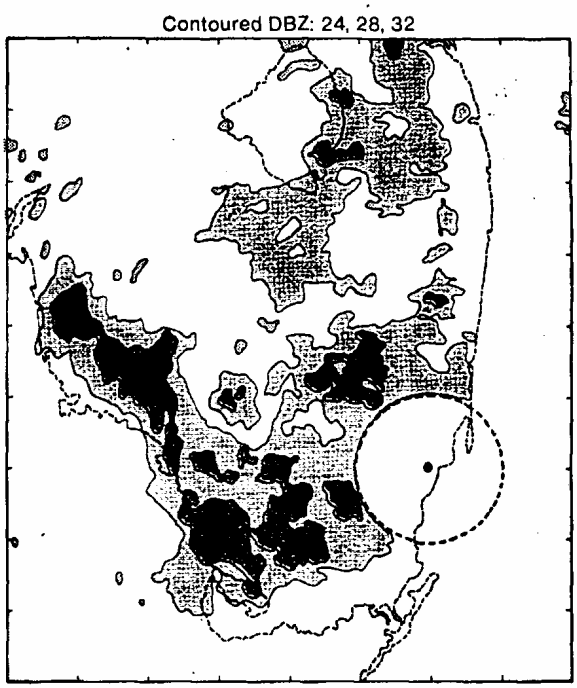

Scale: 27.8 km (15 NMi) per Division
from 1200 to 1500 EDT

(b)

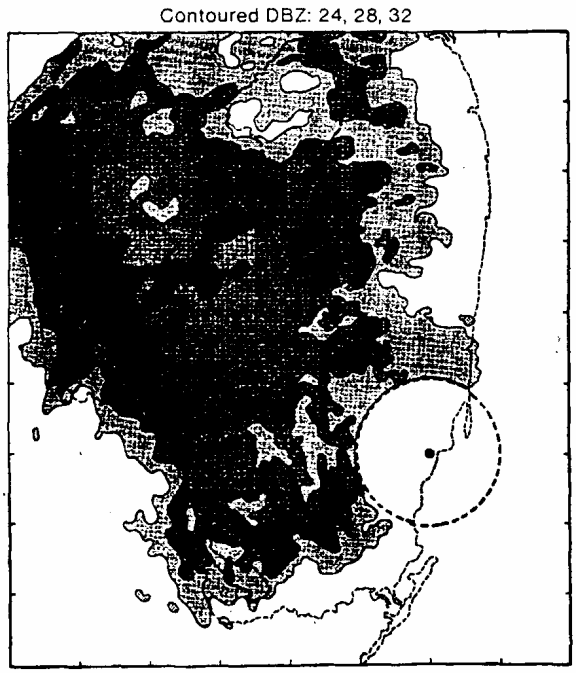

Scale: 27.8 km (15 NMi) per Division
from 1500 to 1800 EDT

(c)

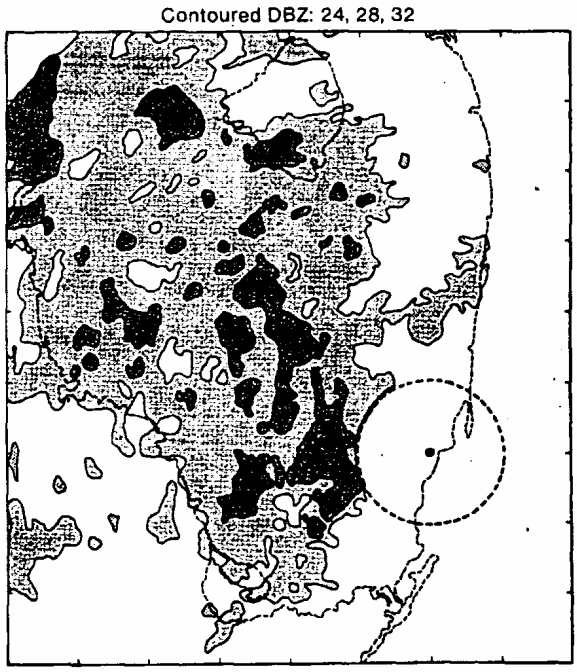

Scale: 27.8 km (15 NMi) per Division
from 1800 to 2100 EDT

(d)

FIG. 2. Convective patterns over south Florida for Type 1 days for (a) 0900–1200, (b) 1200–1500, (c) 1500–1800 and (d) 1800–2100 EDT. Light shading is for radar reflectivities of 24 dBZ, medium shading is for 28 dBZ, and heavy shading is for 32 dBZ.

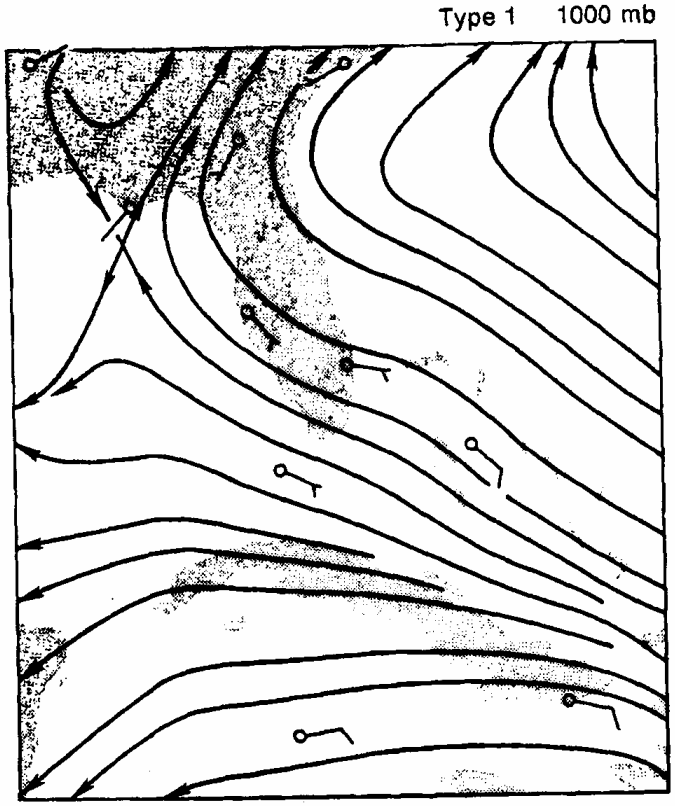

(a)

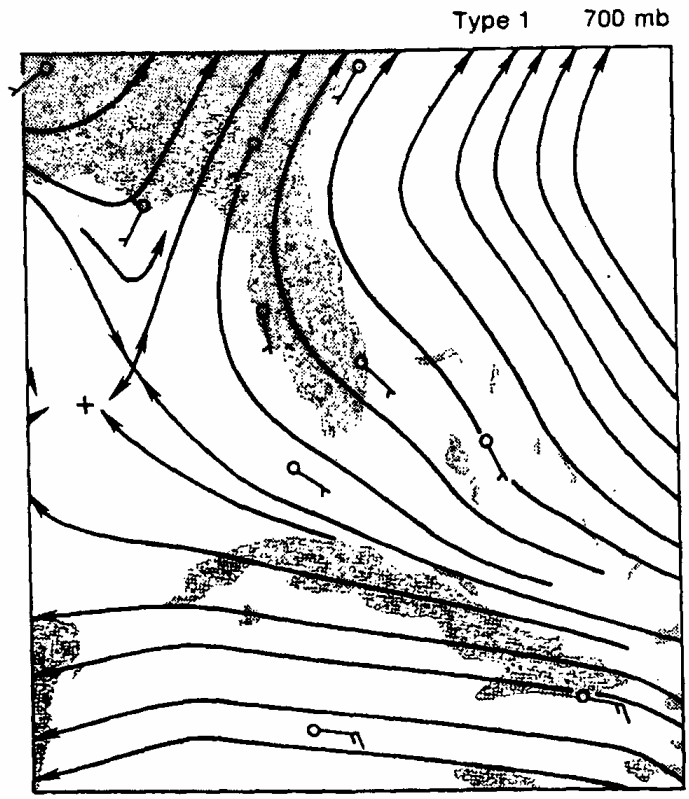

(b)

FIG. 11. Mean synoptic wind field for Type 1 days at (a) 1000 mb and (b) 700 mb. Full wind barbs are 5 m s^{-1} and half barbs are 2.5 m s^{-1}.

Type 1 Days:

Convection is characterized by early development of convection within the east coast sea-breeze convergence zone, followed some time later by convection within the west coast sea-breeze convergence zone. Both sea-breezes advance inland; but the east coast sea-breeze moves faster and farther than its west coast counterpart. Merger of the two sea-breezes usually takes place inland in the center and west of the center of the peninsula. The strongest convection, in the interior of the peninsula, finally begins to diminish during the early evening. Type one days typically have an easterly wind field supported by a east-west ridge from the Atlantic extending over the peninsula. The ridge is an extension of the Atlantic sub-tropical high.

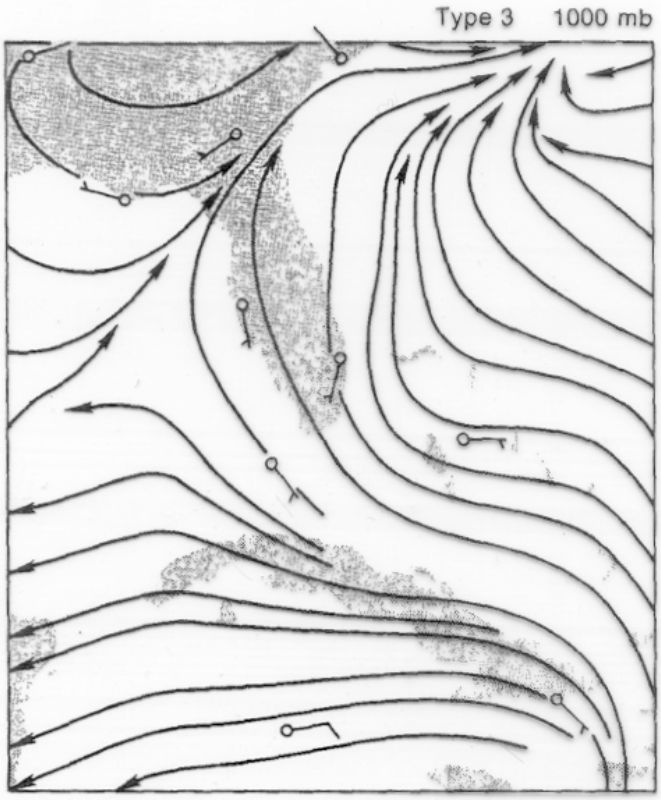

(a)

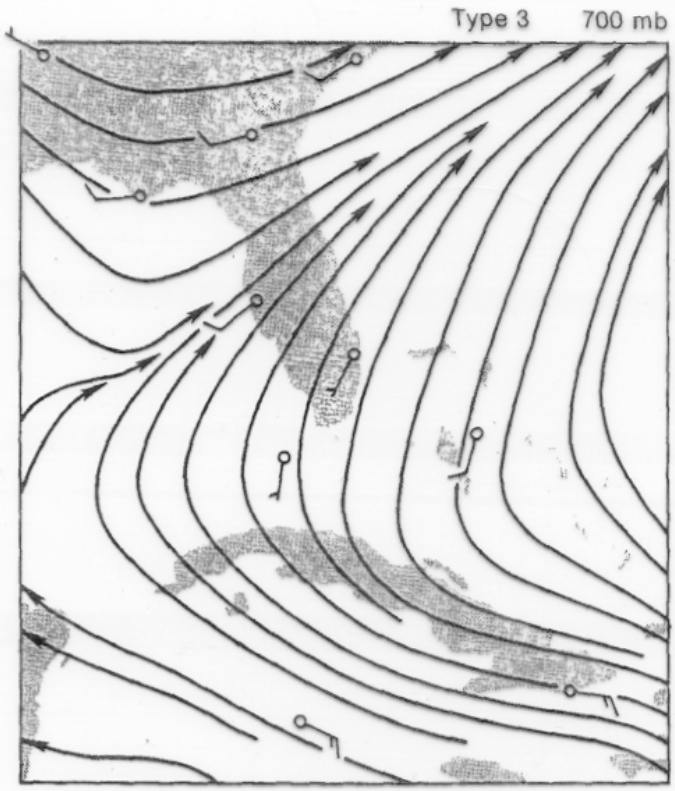

(b)

FIG. 13. As in Fig. 11 but for Type 3 days.

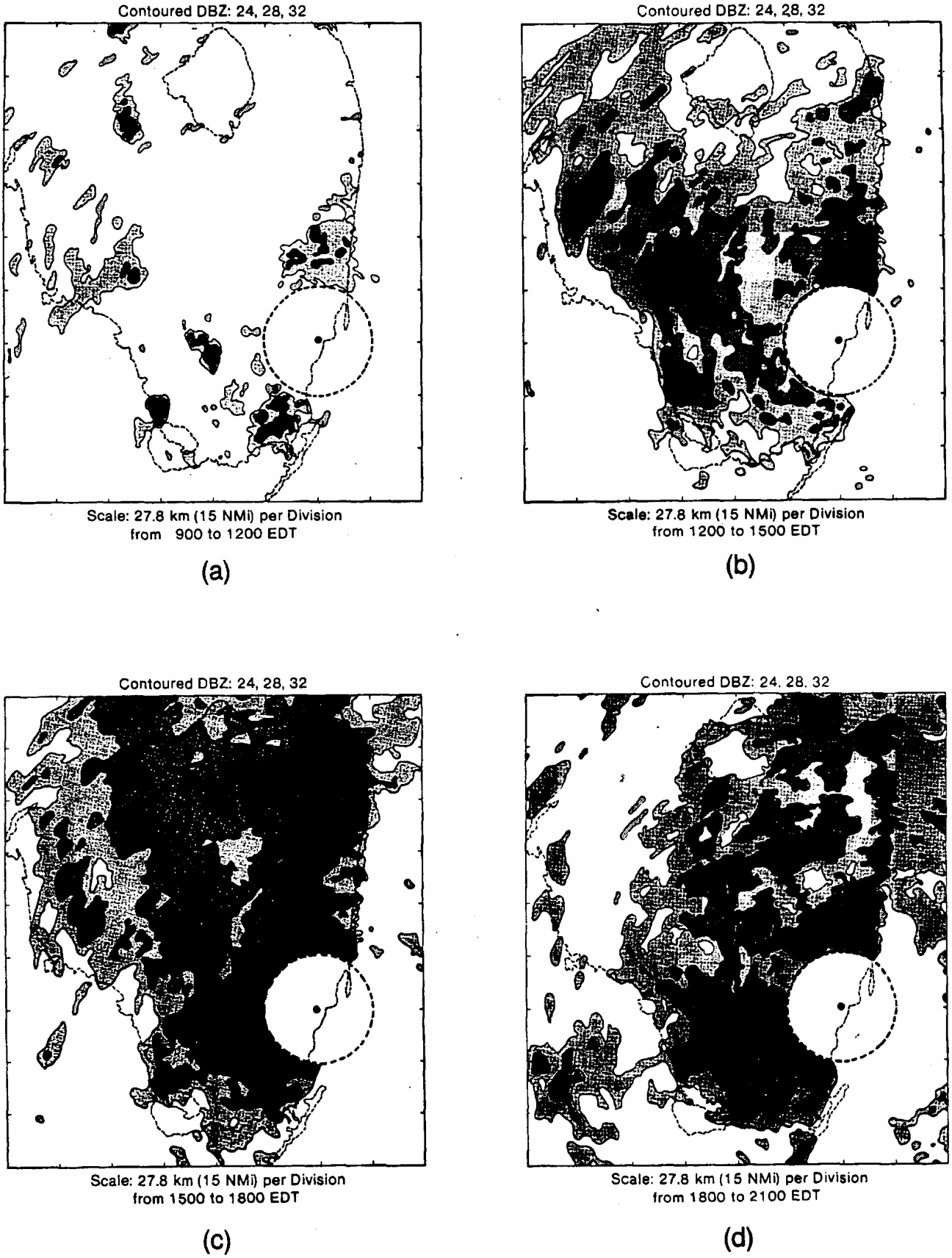

FIG. 4. As in Fig. 2 but for Type 3 days.

Type 3 Days:

Early onset of convection occurs on both coasts. The west coast sea-breeze moves eastward and the east coast sea-breeze remains anchored to the coast. Later in the day the two-convergence zones merge and a strong north-south line of convection forms along the east coast. Compared to the other two regimes, convection is more widespread and dissipation takes place later in the day. The subtropical high in Type 3 days is south of the peninsula resulting in south to southwest flow over the peninsula. A shortwave trough at 700mb is often evident, producing stronger vertical motion and windshear over the peninsula. Type 3 days are not simply a reverse of the easterly flow regimes because, while the sea-breeze evolutions are reversed, the fact the synoptic scale is disturbed alters the intensity and behavior of the convective systems.